Erschienen in: Journal of the American Chemical Society ; 141 (2019), 26. - S. 10120-10136
https://doi.org/10.1021/jacs.9b01883

New Horizons of Nonclassical Crystallization

Marie Jehannin,*[,†,∥] Ashit Rao,*[,‡,∥] and Helmut Cölfen*[,†,§,∥]

[†]Physical Chemistry, Department of Chemistry, University of Konstanz, Universitätsstr. 10, 78467 Konstanz, Germany
[‡]Faculty of Science and Technology, Physics of Complex Fluids, University of Twente, 7500 AE Enschede, The Netherlands
[§]Key Laboratory of Optic-electric Sensing and Analytical Chemistry for Life Science, MOE, College of Chemistry and Molecular Engineering, Qingdao University of Science and Technology, Qingdao 266042, PR China

ABSTRACT: Nonclassical crystallization (NCC) summarizes a number of crystallization pathways, which differ from the classical layer-by-layer growth of crystals involving atomic/molecular building units. Common to NCC is that the building units are larger and include nanoparticles, clusters, or liquid droplets, providing multiple handles for their control at each elementary step. Therefore, many different pathways toward the final single crystals are possible and can be influenced by appropriate experimental parameters or additives at each step of crystal growth. NCC allows for a plethora of crystallization strategies toward complex crystalline (hybrid) materials. In this perspective, we summarize the current state of the art with a focus on the new horizons of NCC with respect to mechanistic understanding, high-performance materials, and new applications. This gives a glimpse on what will be possible in the future using these crystallization approaches: Examples are new electrodes and storage materials, (photo)catalysts, building materials, porous or crystalline materials with complex shape, structural hierarchy, and anisotropic single crystals.

INTRODUCTION

Nonclassical crystallization (NCC) is a generic term for all crystallization processes that do not involve atom, ion, or molecular building blocks as it is the case in classical crystallization.[1] An alternative notation is crystallization by particle attachment (CPA).[2] However, since the building blocks can also be droplets, complexes, clusters, or oligomers, which are not particles, the notation "nonclassical crystallization" is more general and includes these building blocks as well. NCC has a tremendous potential not only to understand complex crystallization scenarios found in nature such as biomineralization or in bioinspired mineralization,[3−5] but also for the synthesis of advanced materials. The reason is that NCC allows for crystal structures, which are not restricted by the constraints of the crystal unit cell anymore as it is the case in a layer-by-layer classical crystal growth. This is illustrated in Figure 1.

Classical crystallization based on layer by layer growth of a primary nucleus/crystal by atom/ion/molecule addition is shown in Figure 1(a), and it is obvious that only crystal faces encoded in the unit cell can grow. This restriction is not valid anymore for NCC, illustrated in Figure 1(b−d). All of these crystallization scenarios involve larger building units with

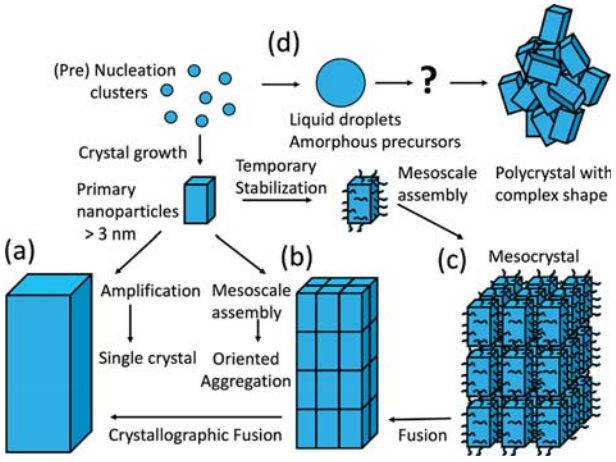

Figure 1. Schematic representation of classical and nonclassical crystallization. (a) Classical crystallization pathway involving layer by layer growth by atom/ion/molecule addition, (b) oriented aggregation of primary nanoparticles forming an iso-oriented crystal, (c) mesocrystal formation via self-assembly of primary nanoparticles covered with organics, and (d) crystallization via liquid droplets or amorphous precursor phases. Please note that the nanoparticles were drawn to the same size for clarity reasons. Partially adapted from ref 6 with permission of the Royal Society of Chemistry.

nanoparticles as the most frequently used ones. Oriented aggregation (Figure 1b) involves the aggregation of nanocrystals in crystallographic register to a superstructure of iso-oriented nanoparticles. These can crystallographically fuse to a single crystal by the process of oriented attachment (OA). If the nanoparticles are colloidally weakly stabilized, they can also self-assemble in crystallographic register by oriented aggregation forming a mesocrystal (abbreviation for mesoscopically structured crystal), with spatially separated nanoparticles in a common crystallographic register (Figure 1c). The mosaic crystal structure shown in Figure 1b is also a mesocrystal, as long as the individual nanoparticles can be distinguished. This shows that mesocrystals can transfer to single crystals by OA, which could be experimentally demonstrated (Figure 7).[7−9] The transformation of liquid droplets or amorphous or sacrificial precursor phases is another NCC pathway (Figure 1d). Here, multiple NCC pathways exist, involving distinct precrystalline entities. For example, for sea urchin spine growth, transformation of a granular phase of amorphous

mineral particles into crystalline calcite via a tortuous propagation pathway by secondary nucleation was suggested,[10] which results in the final mesocrystalline structure.[11] This could also be achieved synthetically for amorphous $CaCO_3$ containing Mg^{2+} by similar mechanisms.[12] Gebauer et al. pointed out the importance of Mg^{2+}, which controls hydration in amorphous $CaCO_3$ and therefore phase transformation in a spatiotemporal manner (see also Figure 12 and corresponding discussion).[13] That way, mesocrystals are obtained by dissolution and recrystallization at the mesoscale, but with ionic dopants, and also polycrystalline or single crystal structures are accessible.[13] There are many other possibilities, which can result in a complex nanostructured crystalline material. The schematic pathways shown in Figure 1 are simplified, and pathways involving clusters, complexes, or oligomers are not shown.

Since crystallization processes can be multistep and multicomponent in nature, incorporating solute clusters, droplets, gels as well as amorphous and crystalline particles,[14] it is important to mention that combinations of the shown pathways are also possible. For example, a nonclassical nucleation event in the prenucleation cluster pathway can lead to nanodroplets, which can subsequently transform into amorphous nanoparticles.[5] These amorphous nanoparticles can crystallize and form a mesocrystal, which can transform to a single crystal via OA. This shows that NCC pathways involve multiple steps (at least 2), opening avenues for control at multiple stages with tremendous outcomes on the final crystal species. Such multistep crystallization is reported for several materials, including colloids,[15−18] clathrates,[19] ice,[20] metals,[21,22] (bio)minerals,[23−28] polyoxometalates,[29] zeolites,[30] proteins,[31−33] amino acids,[34] bioactive molecules,[35] and dyes.[36]

Another advantage of NCC is that it can lead to hybrid materials with enhanced properties. This is especially true for mesocrystals, which are often composed of nanoparticles with their organic stabilizer shells. The organic−inorganic hybrid structure can improve mechanical properties as observed in many biominerals. Biominerals are an archetype for advanced structural design, and it comes as no surprise that NCC plays an important role in bio- and bioinspired mineralization. This will not be further discussed in depth here, and the reader is referred to excellent review articles, which discuss this issue in more detail.[2−4,37]

MESOCRYSTALS

According to the most recent definition, a mesocrystal is a nanostructured and crystallographically ordered material showing clear evidence that it consists of individual nanoparticles in crystallographic register with defined order on the atomic scale in at least one direction, which can be inferred from the existence of an essentially sharp wide angle diffraction pattern.[38,39] Mesocrystals are typical structures and intermediates in NCC (see Figure 1).

Since the introduction of the concept in 2005,[40] mesocrystals found increasing interest due to their unique combination of nanoparticle properties (superparamagnetism, quantum size effect, surface plasmon resonance, catalytic activity, etc.) and often high surface areas with mesocrystal sizes in the micrometer range or even larger. The latter avoids nanotoxicity effects and leads to a much better processability. In addition, mesocrystals are formed by anisotropic nanoparticles and therefore can exhibit directional physical properties (magnetic, optical, electric, etc.), which can be amplified to a different extent in distinct directions. Also, the high inner surface of mesocrystals can be functionally advantageous, and the organic−inorganic hybrid character of many mesocrystals can generate superior mechanical properties.

There are many different ways to synthesize mesocrystals, which are discussed in detail in refs 38 and 39. Currently, 7 different synthesis pathways are known and described: (a) nanoparticle alignment by an organic matrix, (b) alignment by physical forces, (c) crystalline bridges, epitaxial growth, and secondary nucleation, (d) alignment by spatial constraints, (e) alignment by oriented attachment, (f) alignment by face selective molecules, and (g) topotactic (epitaxial) solid phase transformation.[38] There are very likely further synthesis pathways such as particle by particle crystallization of a nanogranular amorphous phase as reported for sea urchin spicules.[10]

These very different formation pathways open up a rich basis for the controlled synthesis of mesocrystals for a large variety of materials. In the past years, significant progress was made in the syntheses of mesocrystals and their applications. A focus was clearly on energy applications and (photo)catalysis, where mesocrystals show superior performance over so far existing materials. This is described in several recent review articles.[41−44] Despite this progress, mesocrystal formation mechanisms are still not well understood. A reason is that ideally in situ techniques working in solution are required, like liquid cell transmission electron microscopy (LC-TEM) or liquid cell atomic force microscopy (LC-AFM). Both techniques can potentially yield detailed insights but have their limitations. AFM can only work on surfaces, and mesocrystal formation cannot be investigated in absence of a surface in solution phase. LC-TEM on the other hand is restricted to the observation of very few building units before the mesocrystal structure becomes too thick to be observed by TEM. Therefore, in situ investigations of mesocrystal formation are rare.

Analysis of Mesocrystal Formation and Structure. The most applied analysis method for the formation of mesocrystals is time dependent analysis of different growth stages by TEM. This can reveal how mesocrystals form and if they are intermediates in an OA process or further topotactic transformations. This was nicely demonstrated for goethite nanoparticles formed from ferrihydrite precursor nanoparticles and subsequently assembled into a mesocrystal, which finally fused to a single crystal (see also Figure 6).[7] Such observations often reveal a multistep formation mechanism as also evidenced for rutile mesocrystals.[45] Here, nanorods form clusters, which then form mesocrystals as intermediate finally resulting in single crystals by OA and Ostwald ripening.[45] However, such TEM investigations are demanding because samples have to be taken at representative reaction stages, which is difficult for fast reactions.

Magnetite/maghemite nanocubes were found to be very suitable to study mesocrystal formation mechanisms since they can be synthesized as defined and monodisperse nanoparticles. The morphology of the truncated nanocubes is very important for the packing arrangement and orientational order in 2 and 3D.[46] The nanoparticles prefer the most efficient space filling packing following a “bump to hollow” packing principle and not only a simple cubic packing as one would expect for the packing of equally sized cubes.[46] This shows that the shape of the nanoparticles is of great importance for the structural

development of a mesocrystal and even small differences in truncations can have a big effect. This puts constraints on the synthesis of nanocrystals purposed for tailoring mesocrystalline architectures.

Grazing incidence small-angle X-ray scattering (GISAXS) characterization of the mesocrystals for nanocubes with different edge lengths also showed a structural dependence.[47] Utilizing a magnetic field during mesocrystal formation allowed tuning of the meso- and microstructure, and it was possible to derive a qualitative phase diagram, which has predictive character for mesocrystal structure and habit for a given nanoparticle size/shape and the applied magnetic field. Such investigations are important in view of mesocrystal applications, which rely on precise structure and organization.

In situ analysis of a mesocrystal is possible with high time resolution using SAXS in a levitating drop coupled with ex-situ SEM for the observation of mesocrystals.[48] These measurements revealed a two-step mechanism for the formation of maghemite nanocube mesocrystals. Upon solvent evaporation and concentration increase, the nanocubes first form densely packed disordered clusters, which transform into mesocrystals at the air−liquid interface and in the solution. This two-step mechanism was confirmed by quartz crystal microbalance measurements with dissipation monitoring.[49] These investigations revealed that the disordered clusters retain certain solvation resulting in a viscous response and that the solvent is released upon mesocrystal formation.

The fine structure of a mesocrystal can also be very precisely characterized using X-ray scattering. Scheele and colleagues were able to quantify the angular correlations between the atomic lattice of the PbS nanoparticles and the mesocrystal superlattice as well as the average orientational misfit due to structural disorder by applying simultaneous SAXS/WAXS measurements at the same location using a nanofocused beam and X-ray cross correlation analysis.[50] Since this technique allows to acquire and analyze several hundred diffraction patterns, the structural analysis is possible on a statistically relevant basis.

All these studies show that a precise characterization of mesocrystals is possible even in a time-resolved manner, which complements the in situ AFM and LC-TEM investigations. Therefore, we can hope to learn more about the mechanisms of mesocrystal formation. This understanding provides the basis for a future tailored design of mesocrystals toward controllable chemical and physical properties.

High Performance Mesocrystals. So far, mesocrystals have found main applications in (photo)catalysis and energy applications. Several recent reviews describe these applications and outstanding mesocrystal performance.[41−44,51] This is based on the high surface area but also on the possibility to expose reactive crystal faces. Therefore, already a great increase in activity can be achieved by realizing mesocrystalline organizations for materials with desirable technological properties. One example is mesocrystalline Pt/Ag alloy as high-performance electrocatalyst with high cycling stability for oxygen reduction reactions due to the surface area and exposure of distinct facets.[52,53]

The most important material for catalytic and energy related applications remains TiO_2. Typical surface areas of the mesocrystals are in the range of 200 m^2/g. Recently, TiO_2 mesocrystal/g-C_3N_4 heterostructures held together by chemical bonds showed enhanced oxidation and reduction abilities compared to TiO_2 mesocrystals, thus a significantly enhanced photocatalytic activity.[54] This can be explained by the formation of a so-called Z-scheme heterojunction, which leads to improved separation of visible light generated electron−hole pairs. This work highlights that the performance of mesocrystals for photocatalysis, and energy applications can even be enhanced by such heterostructures enabling future high performance mesocrystalline materials in these important areas.

It is important to also explore other mesocrystal materials besides TiO_2 in catalysis and energy applications. Recently, $(NiFe)S_2$ pyrite mesocrystals were reported as catalysts for water oxidation.[35] These mesocrystalline materials self-optimized to S-doped metal(oxy)hydroxides upon electrocatalysis with improved performance. This approach is very interesting as it showcases performance improvement by doping. This effect is known for a long time for individual nanoparticles and should therefore amplify the performance of collective organizations such as mesocrystals.

Another recent example of outstanding mesocrystal performance is reported for lithium orthosilicate (Li_2TMSiO_4 with TM = Mn, Fe, Co) as cathode materials for Li-ion batteries.[55] The mesocrystals had a nearly theoretical discharge capacity, superior rate capability, and also a good cycling stability, which suggests such material superstructures as high performance electrode for next generation Li-ion batteries. This outstanding performance could be achieved by shortened Li^+ diffusion paths along the exposed {001} facets as well as a large surface area generated by a hollow mesocrystal structure.[55] This underlines the potential of mesocrystals as outstanding materials in energy and catalysis applications due to the combination of high surface areas and exposure of reactive faces. It is therefore very likely that the performance of mesocrystals in these areas will be much improved due to (a) the increase of surface area, (b) the exposure of reactive facets, (c) the synthesis of heterojunction structures for improved electron−hole pair separation, and (d) the exploration of new materials for mesocrystals, which can replace expensive, rare, or toxic materials in current applications.

Another very promising application area for mesocrystals are mechanical applications. The reason is that mesocrystals allow for organic−inorganic aligned nanogranular structures as they are commonly found in biominerals exhibiting superior mechanical performance like nacre. The reduced grain size as well as the lack of larger cleavage planes and the combination of a ductile elastic organic material with a hard but brittle crystalline material and the precise structural and often hierarchical organization from the nano- to the macroscopic scale are the secrets for its outstanding performance.[3−5] At least on the nano- to micrometer scale, mesocrystals can satisfy these requirements, and therefore, bioinspiration from nature's outstanding materials can be taken.

Mimicking nature's strategies, materials with properties as outstanding as those of the biomineral archetypes can be synthesized. This was demonstrated for nacre, which is the best investigated and most copied biomineral structure.[56] Using the same materials as found in the original biomineral, Yu and colleagues synthesized nacre, successfully mimicking its mesocrystalline structure at the nanoscale.[56] It therefore comes as no surprise that the mechanical properties of synthetic nacre were close to that of the original biomineral. This impressively demonstrates that it is possible to mimic the structure of biominerals. Since many of them are mesocrystalline or have nanogranular organic−inorganic hybrid struc-

tures,[4] it is interesting to explore whether the structure of a biomineral can be transferred to another material class under preservation of the outstanding hierarchical design.

This was recently shown for calcium silicate hydrate (CSH), the binder of cement, which is of central importance for the construction industry.[57] This result is surprising because CSH is known for its immediate nonspecific binding due to its function as binder in cement. This results in random networks of the primary CSH nanoparticles thus decreasing the mechanical strength. Inspired by the mesocrystalline sea urchin spine[11] and using synthetic polymers with binding motifs previously identified by a phage display approach,[58] CSH mesocrystals were realized with interspacing polymer between the CSH nanoplatelets.[57] The mechanical properties of these mesocrystals were close to those of nacre demonstrating the possibility to adapt material design concepts from nature to synthetic materials.

Another recent development is the construction of mesocrystals consisting of metal organic framework (MOF) nanoparticles. MOFs are well-known for their exciting properties and good performance in gas sorption/separation, catalysis, and energy devices due to their high surface area as well as tunable pore size and structures. Therefore, combining the concept of MOFs with that of mesocrystals is attractive for the design of high-performance materials with all positive MOF properties but additionally also the easy and fast accessibility of the MOF pore structure through the pores in a mesocrystal. Such mesocrystals were recently reported by Schmidt et al., who synthesized MOF mesocrystals regulated by double hydrophilic block copolymers (Figure 2).[59] They synthesized mesocrystals from a Zn^{2+}/Cu^{2+} based MOF using a poly(ethylene oxide)-block polymethacrylic acid double hydrophilic block copolymer. A mesocrystal composed of hexagonal nanorods was obtained as a kinetic polymorph. Using longer ethylene oxide blocks led to plate formation instead of rods, demonstrating that the structure evolution relies on mutual interactions between functionalities of the polymer and of the MOF. Changing the solvent to the polar protic solvent methanol induced a polymorphic transformation to a tetragonal mesocrystal as the stable polymorph.[59] This is an important finding as different polymorphs have dissimilar properties. It also indicates that mesocrystals can behave similarly to classical crystals with the difference that their building blocks are larger.

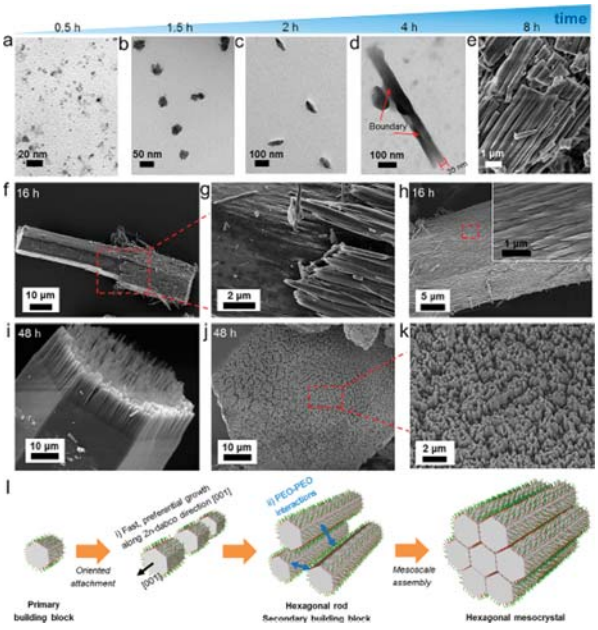

Figure 2. Growth processes of hexagonal rods mediated by EO68MAA8 at molar ratio of [COOH of EO68MAA8]/[Zn^{2+}] = 4, mass ratio of PVP/EO68MAA8 = 1.5, and 120 °C. (a–k) Time-dependent TEM and SEM observations after reaction for 0.5 (a), 1.5 (b), 2 (c), 4 (d), 8 (e), 16 (f–h), and 48 h (i–k). (l) Proposed growth mechanism. Image reproduced from ref 59 with the permission of the American Chemical Society.

Protein Mesocrystals. A very exiting recent development is protein mesocrystals. Yang et al. reported that lysozyme unfolds after reduction of the disulfide bonds and rearranges into short β-sheet aggregates and nanostructures with crystalline lamellar core and amorphous protein shell.[60] This process was followed by mesoscale self-assembly to a mesocrystal. Finally, fusion of the nanocrystals led to single crystals.[60] Mesocrystals were also formed by stacking of single crystalline protein sheets. It is yet unclear how general this approach is but if mesocrystals can be formed by various proteins, exciting applications may arise because of the prospects of biochemical multifunctionality, substrate channeling, and tunable responses.

Another exciting possibility is to use a hybrid between a protein and a mesocrystal. Coupling the enzyme laccase (LAC) to Cu_2O nanowire mesocrystals (Figure 3) by protein

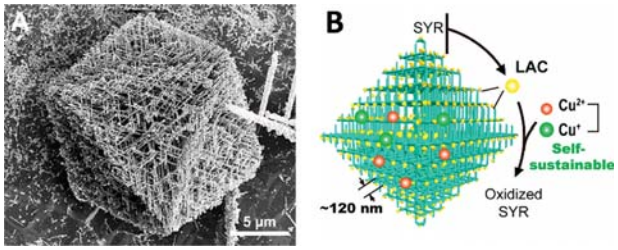

Figure 3. (A) SEM image of single and large-area LAC-Cu_2O mesocrystal. (B) Schematic representation of the oxidation of a model compound SYR by environment-responsive Cu^+/Cu^{2+} ion-regulated enzyme activity. Image reproduced from ref 61 with permission of the American Chemical Society.

immobilization and covalent binding, outstanding catalytic performance of the enzyme hybrid mesocrystal was achieved, which was 10-times higher than that of the enzyme.[61] Laccase is a copper containing enzyme and is activated by Cu^+ and Cu^{2+} with a higher activity for the Cu^+ activation. Since the Cu_2O nanorods forming the mesocrystal continuously undergo a dissolution-recrystallization process, Cu^+ is released and partially oxidized to Cu^{2+} ions, available for enzyme activation. Ion release and the related Cu^+/Cu^{2+} ratio are pH dependent factors. In addition, the open architecture of mesocrystals providing a high surface area is important for the observed superior enzymatic activity. This work has potential for the further development of high-performance nano-biocatalysts.

Binary Mesocrystals. From the above examples, the advantages of mesocrystals become clear. However, the potential of mesocrystals is even larger, if binary mesocrystal structures self-assembled from two different nanoparticle species can be realized. This could be nanoparticles with different sizes and/or shapes and/or chemically different

nanoparticles. That way, the properties of the individual nanoparticles could be combined in one material in a directionally dependent way and emergent synergistic properties/effects are also expected from the mesocrystal superstructure and the action of the nanoparticle lattice.

It is, however, not easy to realize such structures since the surface chemistry of the nanoparticles needs to be tuned in a way that mesocrystals with any composition of the two building blocks can be realized without phase separation into two individual mesocrystals. In addition, the size ratio and the shapes of the nanoparticles need to be matched, which requires highly defined nanoparticle syntheses.

Imai and co-workers were the first who obtained a binary 2D mesocrystalline film of Pt and $BaTiO_3$ nanocubes both stabilized by oleic acid (see Figure 4).[62] The mesocrystal

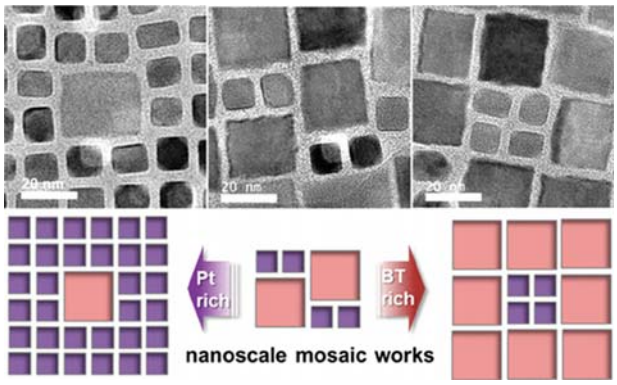

Figure 4. Binary 2D mesocrystals composed of 10 nm Pt and 20 nm $BaTiO_3$ nanocubes. The structure of the binary mesocrystals can be tuned by varying the nanoparticle composition. Image reproduced from ref 62 with permission of the American Chemical Society.

structure varies with the composition of the nanocube mixture (Figure 4). Due to a slight variation in nanoparticle size and shape, the formed tetragonal mesocrystal arrays were slightly distorted with occasional vacancies and edge dislocations highlighting the demands for synthetic approaches toward well-defined nanoparticles.

This first example shows that binary mesocrystals are feasible. It can be expected that future research will be directed to the more demanding synthesis of 3D mesocrystals. Also, it will be highly interesting to learn about the physical and chemical properties of binary mesocrystals. These exiting structures are considered to have the highest future potential among mesocrystalline structures due to the combined functionality of multicompositional nanoparticles, for instance providing the exploitation of synergetic effects at the nanoscale.

Mesocrystal Networks and Intermediates to Single Crystals. The above examples show that the potential of mesocrystals to be utilized has just started to be exploited. In fact, the structural and application possibilities of mesocrystals are much larger than initially anticipated.[1,40] A further very interesting possibility is to induce a partial fusion of the nanocrystals typically via mineral bridges. In a sophisticated electron microscopy work, Rosseeva et al. demonstrated that in mesocrystals formed by oleic acid stabilized PbS nanoparticles, fibrillar oleic acid structures guide the mineralization of PbS to form mineral bridges in between the oriented nanocrystals in the mesocrystal (Figure 5).[63] Mild annealing further promoted the formation of mineral bridges.

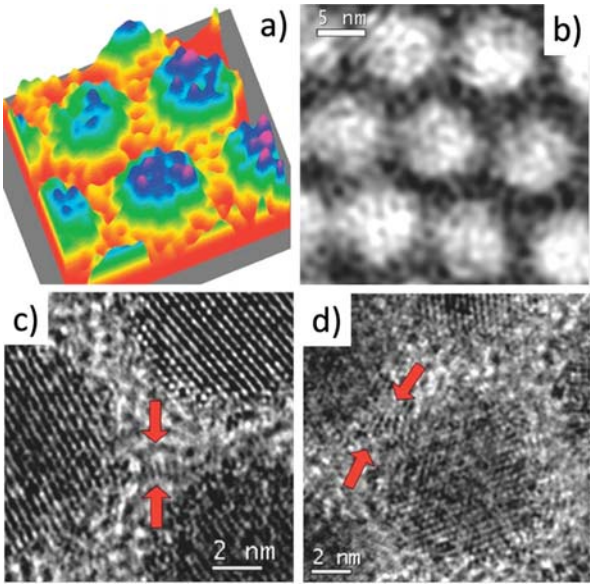

Figure 5. 3D representation of the phase image retrieved from a TEM electron hologram. (a) Color code corresponds to about 4 nm height from green to blue. Bridging organic fibrils appear in yellow. (b) 2D representation of phase image retrieved from the electron hologram. Lateral resolution is about 0.4 nm. PbS nanoparticles and interconnecting subnanometer oleic acid fibrils appear bright. Most often there are between two and four nodes interconnecting neighboring nanoparticles. (c, d) Conventional high-resolution TEM of thin PbS bridges interconnecting the PbS nanoparticles (red arrows). Image reproduced from ref 63 with permission of Wiley-VCH.

This work demonstrates that it is possible to crystallographically connect the aligned nanocrystals in a mesocrystal forming a nanoparticle network. This is highly interesting for electronic applications since this strategy allows for the connection of metal or semiconductor nanoparticles.[63] The potential is even higher for binary mesocrystals. It has been demonstrated for TiO_2 mesocrystals with reduction induced defect states that so-called hot electrons with energies lower than the Schottky barrier height could be transferred to the semiconductor from proximal Au nanoparticles.[64] This can boost plasmonic photocatalyst efficiency and application. Indeed, broad band Vis-NIR light harvesting for photocatalytic H_2 production could be achieved by attaching Au-nanorods to TiO_2 mesocrystals.[65]

Taking a broader view, electronic contact between metals and semiconductors can lead to self-assembled electronic nanocircuits via a bottom up approach. The advantage of such structures would be their largely variable composition and structure as well as easy synthesis of 2D mesocrystal films by Langmuir–Blodget film deposition, spin coating, or simple solvent evaporation even on large scale.[38]

Mesocrystals are no thermodynamically stable species due to their large inner surface areas, which can in the best case be kinetically stabilized. This means that an inherent thermodynamic driving force exists to minimize the inner surface by crystallographic fusion of the already iso-oriented nanocrystals simultaneously gaining lattice energy. Therefore, mesocrystals can serve as intermediates in an OA process, which involves multiple steps as schematically shown in Figure 1. Penn and co-workers demonstrated that ferrihydrite precursor nano-

particles transform to goethite nanoparticles, which then subsequently form elongated mesocrystals (Figure 6a). Upon

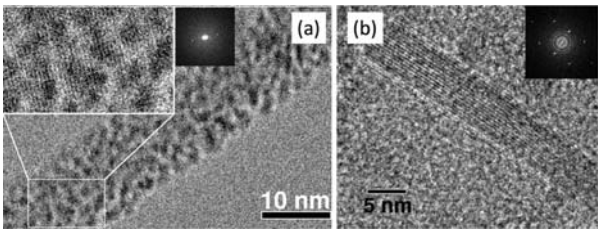

Figure 6. High-resolution TEM images of goethite mesocrystal intermediates in an OA process. Shown by cryo-TEM, (a) the mesocrystal intermediate is composed of individual nanoparticles surrounded by a water shell and (b) the single crystal after OA of the mesocrystal intermediate. Reproduced from ref 7 with permission of the American Chemical Society.

further aging, crystallographic fusion of the iso-oriented nanocrystals occurs eventually forming goethite single crystals with the same orientation of the long axis as the mesocrystal intermediate (Figure 6b).

■ ORIENTED ATTACHMENT

First reported by Penn and Banfield for titanium dioxide, oriented attachment (OA) is nowadays accepted as a widespread nonclassical growth mechanism.[66,67] It refers to a "match-and-dock" mechanism, where primary particles attach and fuse to one another on specific crystal faces with an alignment of their crystallographic direction (see also Figure 1b).[68,69] From a thermodynamic point of view, OA is favored by the decrease of the surface energy as the primary particles merge into a single crystal.[70] OA plays a role in biomineralization and has been reported in the formation of synthetic crystals including gold, silver, metal oxides, or semiconductors.[71,72] OA enables to synthesize single crystals with well-defined size, usually with dimensions of tens of micrometers, having few up to no defects, due to the fast diffusion of dislocations at the surface of the building blocks.[73] In the past decade, the development of analytical techniques like LC-TEM enhanced the knowledge of different steps occurring during OA. However, the detailed understanding of the forces involved in each step is still missing. In this part, we will focus on the influence of the different interparticle forces during OA. For a detailed understanding of the OA kinetics, the reader can refer to the excellent review by Xue et al.[74]

Ligands Modulate OA. For OA to occur, the primary particles have to be stable toward other growth mechanisms, such as Ostwald ripening, on a time scale longer than the attachment process. Hence, the nanoparticles involved in OA are often stabilized by ligands, surfactants, or polymers. Such additives may greatly influence particle OA either by modifying the morphologies of the primary building blocks during their synthesis or by impacting interparticle interactions during their assembly. PbS nanoparticles, synthesized in the presence of chloroalkanes, assemble in a 2D manner into single crystal nanosheets.[75] The building blocks are 3 nm truncated cuboctahedra, which attach via {110} facets. Additives can stabilize highly reactive faces, which further bind to each other by OA. Similarly, PbSe primary particles attach either on the{100}, {110}, or {111} crystal facets, depending on the mixture of surfactants added during their synthesis, producing nanowires with different morphologies (Figure 7).[76] The authors proposed that OA is driven by the nanoparticle's

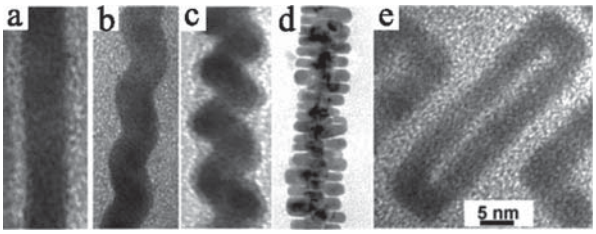

Figure 7. PbSe nanowires and nanorings grown by OA in different surfactant mixtures. (a) Straight nanowire synthesized with oleic acid and *n*-tetradecylphosphonic acid. (b) Zigzag nanowire grown in the presence of hexadecylamine (HAD). (c) Helical nanowire from an oleic acid/HAD/trioctylamine mixture. (d) Branched nanowire formed in the presence of primary amine. (e) Hexadecylamine and diphenyl ether additives lead to nanorings. Reprinted with the authorization of the American Chemical Society from ref 76.

internal dipole moment, arising from the difference in electronegativity of the lead and selenide terminated {111} facets. The dipole moments would then drive growth directions and final morphologies of the nanowires.

Elementary Steps. Li et al. were the first to directly observe the OA of iron oxide nanoparticles by LC-HRTEM.[9] A three-step process was revealed consisting of an alignment step, contact and fusion of the two particles (see Figure 8).

During the alignment step, two particles come to close contact, detach, and rearrange repeatedly until the orientation of the crystal lattices matches. Up to that stage, the particles always remain separated by at least a nanoscale solvent layer. Once aligned, the particles jump to contact and finally fuse, by an atom by atom reorganization at the interfacial region. Such OA pathway is sometime referred to as the prealignment pathway. In the case of citrate-capped gold nanoparticles, similarly, the OA occurs by alignment of the particles followed by their jump to contact.[70] The particles rotational speed differs during these two steps. First, as the {111} facets are largely misaligned the particles rotate randomly. As the particles access a configuration with a lower misalignment, the particle's separation distance shrinks below twice the ligand size, the capping layers interpenetrate and θ decreases until the facets are perfectly aligned. As they are separated by a ligand monolayer, the particles jump to contact. Both the increase of the particle rotation speed and their jump to contact reveal the existence of direction-specific interactions. The forces at the origin of the direction-specific interactions are a matter of debate. For the self-assembly of gold nanocubes, an alternative attachment pathway has been observed simultaneously to the prealignment pathway.[77] The particles first connect in a misaligned configuration, usually by the connection of two particle edges. The particles further rotate around the attachment point until their faces are aligned. To our knowledge, the occurrence of this postalignment attachment pathway is rarer than the prealignment pathway.

An alternative pathway toward single crystals is named random attachment (RA). In that case, nanoparticles first fuse into a polycrystal. The crystallographic reorientation further occurs via rotation, and material redistribution.[78] Crystallographic reorientation may occur spontaneously or be induced by external forces. For example, the aggregation of vaterite nanocrystals can lead to a "single crystal" with a polycrystalline

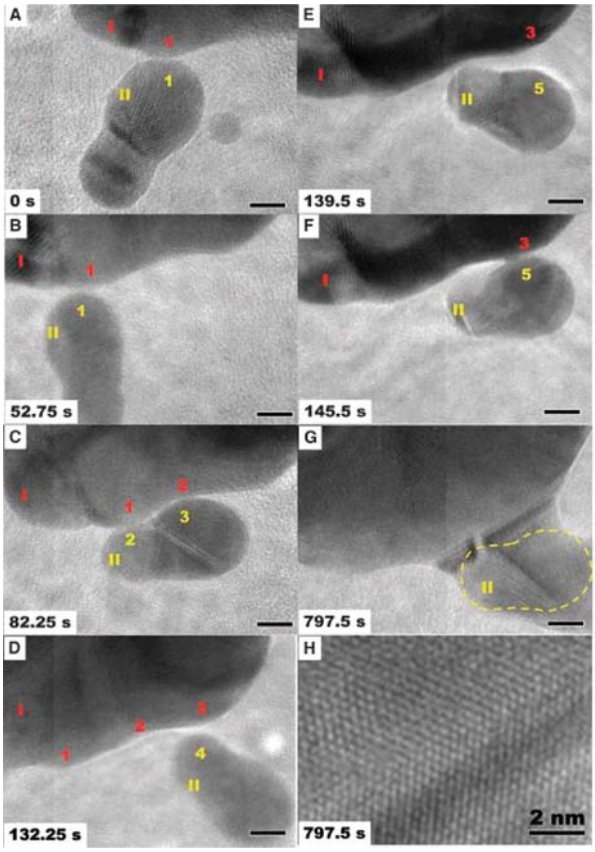

Figure 8. LC-TEM image sequence of OA between two iron oxyhydroxide particles. Particles I and II initially contact repeatedly in misaligned configurations and rearrange during the alignment step (A–D). As the particle crystal lattices match (E), the particles jump to contact (F) and fuse (G, H). Scale bar: 5 nm. Reprinted with the permission of AAAS from ref 9.

surface of 5 nm grains.[79] The surface transforms into a single crystal following exposition to high pressure. This finding indicates that surface stress can induce crystallographic lattice alignment.

Interactions at the Origin of OA. Up to now, the detail of the interactions leading to OA remains unclear. It has been alternatively attributed to Coulombic, van der Waals (VdW), or solvation/hydrophobic forces. OA reduces the total surface energy of the system. It has long been assumed that this surface reduction was the unique thermodynamic driving force behind OA and that consequently, OA should preferentially occur between the crystals faces having the highest surface energy. However, this theory was contradicted by experimental evidence of OA occurring on low energy surfaces. Zhang et al.[69] postulated that OA was driven by both the surface energy and interatomic interactions of the particles. On the basis of this idea, they used molecular statistic calculations to successfully predict the OA direction of approximately 30 crystals. By calculating the VdW and Coulombic contributions for SiO_2, ZnS, and ZnO crystals, the authors showed that the Coulombic interactions dominate the approach of the primary particles as soon as the particles are in close proximity.[80] Thus, Coulombic forces were found to govern the attachment direction. Although the developed model correctly predicts the faces on which OA occurs between two particles, it does not explain mechanisms by which the crystallographic directions align. Adapted from colloidal probe AFM, dynamic force spectroscopy (DFS) performed with a single crystal tip measures interparticle interactions as a function of the crystal's relative orientations. In aqueous solution, the attractive force between one $(000\bar{1})$ terminated ZnO substrate and a manufactured (0001) ZnO tip exhibits a 60° periodicity as a function of the relative angle between the crystal faces.[81] During the tip retraction, the largest attractive force occurs as the two lattices are in perfect alignment (rotation angle of 0° or 120°) or misaligned by 60°. The adhesion free energy of the ZnO tip and surface increases linearly with the contact surface area. The 60° periodicity was confirmed by potential mean force (PMF) calculations, obtained through molecular dynamics (MD). For all the relative orientations, the simulation reveals three local energy minima (at interparticle distances of approximately 5.8, 7.5, and 9.7 Å), attributed to a structuring of the interlaying water molecules. At relative orientations of 0°, 60°, and 120°, the first minimum (5.8 Å) is largely negative, whereas for other orientations, the global energy minimum corresponds to the second well (7.5 Å). The structuring of interparticle water layers would keep the particles separated when they are in a misaligned state.

In a solution, the competitive interactions between particles, solvent, and ligands make it challenging to isolate the individual contribution of the different forces. Zhang et al.[82] combined in a single experiment AFM based dynamic force spectroscopy and environmental TEM (ETEM) technologies to isolate the VdW contribution of the particle–particle interaction. This configuration enables precise measurement of tip–surface distances. ETEM-AFM measurements were performed between two (001) TiO_2 faces for different water vapor pressures. During the tip–surface approach, the interactions are independent of the crystal lattice alignment. However, an angular dependency was measured during the retraction, with the larger attraction measured as the crystal lattices are perfectly aligned (Figure 9). The attraction decreases as the azimuthal angle between the TiO_2 faces increases and reaches a minimum for the maximum misalignment at $\theta = 45°$. As the vapor pressure increases, the force becomes weaker, but its direction of variation as a function of the azimuthal angle persists.

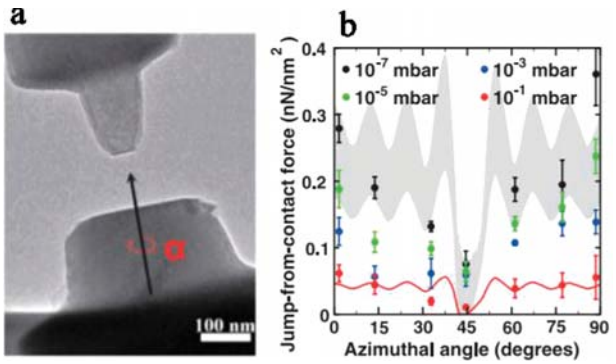

Figure 9. (a) TEM image of the TiO_2 tip and substrate used for ETEM-AFM measurements. (b) Jump-from-contact forces measured as a function of the azimuthal angle at different vapor pressures. The gray domain corresponds to the VdW forces calculated using the Lifshitz theory. Adapted with permission of AAAS from ref 82.

Calculation of the VdW forces using the Lifshitz theory agreed with the measured attraction. The authors proved that VdW forces of crystalline material can be sensitive to the relative particle orientations. VdW forces could be a key factor in the alignment of crystal faces. The question remains if other forces, as Coulomb forces, may also be orientation specific and thus contribute to the alignment during OA. Up to now, the studies focus on the oriented attachment of particles composed of the same material. However, one could imagine to grow binary crystals by the OA of building blocks made of different materials, with a similar crystalline structure.

High Performance Crystals from OA. Nanocrystals are often considered as perfect and free from crystal defects such as dislocations. Indeed, defect removal is favored by the short diffusion length necessary for the defect to reach the crystal surface and thus amplified near the crystal surface.[73] In the case of PbTe nanocrystals, dislocations introduced during the OA of the particles on the {100} facets diffuse to the crystal surface in tens of seconds.[73] Taking advantage of fast defect removal, OA enables to synthesize crystals with few defects and superior performance for diverse applications as catalyst, photovoltaic cell, gas sensor, or for depollution.

Up to now, the energy sector has most examples of high-performance crystals synthesized by OA. This is partly explained by the higher mobility of electrons and charges in these single crystals with low defect density. Using a process related to OA, designed as topotactic oriented attachment (TOA), Kim et al. successfully produced perovskite films exhibiting a carrier mobility nearly 3 times higher than that of conventional polycrystalline perovskite films.[83] The uniaxially oriented film is synthesized by spin coating precursors on a TiO_2 surface. Annealed at 130 °C, the precursors attach along their [111] direction during their topotactic transformation to perovskite, which leads to uniaxially oriented perovskite films with higher carrier mobility. Such film is a promising candidate for applications as optoelectronic components including solar cell materials. The enhanced mobility of charge carriers is also a significant advantage for catalysis. The oxygen reduction reaction (ORR) is highly relevant for several renewable energy sources as fuel cells or water splitting.[84] However, aggregation of Pt-based nanoparticles is an obstacle to the design of highly efficient systems.[85] Ma et al. used a solid state method to synthesize different Pt-based nanowires.[86] Using HRTEM equipped with a gas cell holder, the authors showed that after an initial growth of the nanoparticles by atom addition, they later fuse into oriented nanowires by OA. The Pt−Ni system exhibits a high mass catalytic activity for the ORR, which is 10 times higher than that of the commercially available Pt/C system.

Besides, a 3D network grown by OA often exhibits porous structures, which is significantly advantageous for high-performance materials. Solid state dye sensitized solar cells are composed of a hole transport material loaded on a TiO_2 mesoporous support. Tétreault et al. developed a 3D network of TiO_2 nanowires synthesized via OA during hydrothermal transformation of nanorod precursors.[87] In addition to a higher conductivity, compared to the nonoriented TiO_2 support, the oriented TiO_2 network exhibits large pores, which enable multiple light scattering inside the material and enhanced light harvesting. This material achieved a conversion efficiency of nearly 5%, comparable to the efficiency obtained for solid state dye sensitized solar cells. Such porous structures have also proven to be beneficial in the field of lithium-ion batteries. Wang et al. synthesized SnO_2 nanosheets, with a thickness around 2 nm, by a one pot hydrothermal synthesis[88] and demonstrated that the nanosheets resulted from the OA of nanocrystals.[89] After 50 charge−discharge cycles, the SnO_2 nanosheets exhibit an extremely high reversible capacity of 543 mAh/g, which is attributed to both the extremely low thickness of the nanosheets, which shortens the diffusion path of the ions trough the material, and the porous network, which can adapt to reaction volume changes. For comparison, after 50 discharge−charge cycles, the reversible capacity of SnO_2 hollow spheres and nanoparticles are 355 mAh/g and 177 mAh/g, respectively.[89]

The OA pathway also enables to synthesize anisotropic materials, with new properties compared to the bulk material. For example, WO_3 is usually not active toward CO_2 reduction. However, WO_3 nanosheets reduce CO_2 into CH_4 in the presence of water.[90] The photocatalytic activity of WO_3 nanosheets is due to a quantum size effect as one of the solid dimensions approaches the Bohr radius of the material. OA is an efficient bottom-up approach to synthesize 1D or 2D nanomaterials. As this pathway can drastically increase crystal performance and with the growing understanding of interactions leading to OA, it is expected that crystals obtained from OA will continue to garner a lot of attention in following years.

SHAPING CRYSTALS WITH AMORPHOUS PRECURSORS

Crystallization pathways navigate complex energetic landscapes to converge upon the final phase and structure. Key participants are often noncrystalline entities with distributions of size, structure and solvation intermediate to those of fundamental solutes and emergent crystals. These precursors greatly impact emergent crystal morphologies, nanostructures and organizations. For instance, during mineralization, prior to establishment of solid/liquid or liquid/liquid interfaces, the fundamental solute units can form dynamic, self-associates termed as clusters, existing in equilibrium with unbound units.[24,91] With increasing supersaturation, the association of free and associated species, accompanied by internal condensation and solvation loss, leads to the separation of solute lean and solute rich (liquid condensed) phases.[25,26] Originating from this miscibility gap, unless extrinsically stabilized, the liquid condensed phases (LCPs) can undergo solidification, yielding amorphous and crystalline nanoparticles or contributing to growth of preexisting particles (Figure 10).[23,25,92,93] Even during the nucleation of metal nanocrystals from the spinodal regime, the separation of solute-rich and solute-poor liquid phases is identified as an intermediate step (Figure 10).[21] Along the reaction coordinate, amorphous clusters initially form within the enriched fluidic phase, undergoing further desolvation and molecular reorganization to form nanocrystals. Crystallization reactions recruiting amorphous intermediates also encompass organic materials, ranging from small molecules to macromolecules.[33,34,94,95] For instance, during crystallization of DL-glutamic acid monohydrate, the structural relaxation and desolvation of highly hydrated nanoscopic species are rate-determining steps (Figure 10).[34] Even protein crystallization involves transitions from clustered species and liquid condensed phases to ordered assemblies.[31,32] In this manner, crystallization schemes recruit a multiplicity of distant and immediate precursors and extend well beyond an exclusive mediation by classically considered

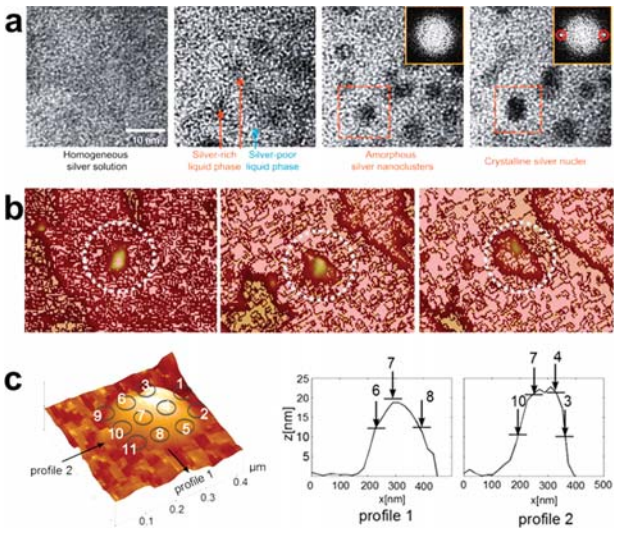

Figure 10. (a) Nucleation of silver nanocrystals involving demixing into silver ion-poor and -rich liquid phases, with the latter forming intermediate amorphous nanoclusters. (b) Encircled nanodroplet transforming into a new crystalline layer on a Glu·H_2O crystal. (c) Gel-like precursor on a calcite surface with corresponding height profiles. Reproduced with permissions from (a, b) Springer Nature and (c) American Chemical Society from refs 21, 34, 93.

"critical nuclei".[5] Thermodynamic and kinetic factors govern the relative extent of participation, i.e., the transitions and stabilities of these solute, fluidic and particulate constituents in crystal nucleation and growth, thereby providing selective accessibility toward the ensemble of nonclassical schemes.[2,95−97] Relative to NCC recruiting nanocrystalline building units, the transitions of solid and liquid-like amorphous phases toward crystalline architectures are less understood (Figure 1d). However, fluidic and particulate amorphous phases enable the intimate coupling of phase transformation reactions with particle attachment and assembly. Due to low densities and slow sedimentation, the interactions of amorphous phases can be kinetically suppressed, enabling to synergistically control attachment/coalescence and phase transformation. On the other hand, the diffuse interfaces and high solubility of amorphous phases increase the probability of uncontrolled attachment or fusion. Nonetheless, with suitable additives and reaction conditions, amorphous phases can be effectively directed toward intricate crystal architectures.[37,95]

Stabilization of Amorphous Precursors. In view of the metastable nature of amorphous precursors, nucleation and crystallization studies performed in well-defined chemical environments are particularly illuminating. Since amorphous phases are susceptible to alterations via solvent turbulence, shear forces, inhomogeneous mixing as well as irradiative stress, the assignment of either binodal demixing or spinodal decomposition for related phase separation phenomena is nontrivial. For instance, prolonged electron irradiation induces the agglomerative deformation of amorphous particles,[13] suggesting that perceived particle morphologies do not fully reflect the related mechanisms. Second, amorphous (solvated) inorganic constituents typically present low electron contrast, rendering their microscopic distinction from applied stabilizers at the nanoscale a challenge.[98] However, in defined chemical media, prior to the nucleation of solid phases, time dependent THz absorption spectroscopy identifies distinct variations in water dynamics, underpinning a liquid−liquid binodal event for nanodroplet formation.[23,25] Anionic polymers appear not to influence the binodal limit for the phase separation of fluidic minerals; however, they can invoke the local accumulation and stabilization of cluster species and LCPs, inhibiting the nucleation of solid particles.[25,99,100] Under these conditions, liquid-like precrystalline phases amenable to physicochemical manipulation are realized.[25,92,99] For instance, stabilized by charged polymers such as poly(acrylic acid) and poly(aspartic acid), distinct crystal precursors are termed as "polymer induced (or stabilized) liquid precursors" (PILPs).[100,101] Considering the moderate Ca^{2+} ion binding capacity of poly(acrylic acid) (i.e., about one cation/five carboxylic acid groups),[99] the stabilization of malleable crystal precursors does not solely depend on ion complexation. Proposed comechanisms include local buffering related bias toward bicarbonate ions as well as the roles of polymer- and ion-associated local hydration in suppressing dehydration and deprotonation events, essential for the subsequent establishment of crystalline phases.[13,23,25] Analytical investigations on polymer- and protein-stabilized mineral LCPs also reveal significant fractions of (bio)polymers excluded by the precrystalline phase.[101,102] In certain scenarios, these stabilizers adsorb to the liquid−liquid or liquid−solid interfaces, transiently stabilizing precrystalline droplets or amorphous derivatives via nanoscopic confinement.[97,103] Functioning as adsorbates, these molecules modify phase interfaces, akin to the roles of nanocrystal-capping agents in tuning VdW and electrostatic forces between interacting bodies. Stabilizers, excluded from the precrystalline material as well as the interfaces of precrystalline phases, are equally functional during nucleation and crystallization in modulating depletion stabilization and interdroplet/particle interactions.[101,102] With lower contents of these stabilizers, reactions can intermittently undergo de-emulsification and produce fluidic precrystalline phases.[25,92] In nature, these depletion forces greatly impact crystallization reactions, wherein typically 20−30% of the volume of biological environments is occupied by macromolecules. Evidence comes from the relation between the supersaturation levels required for nucleation and the fractional volume occupancy of applied (bio)polymers, bringing forth the concept of a "Goldilocks effect" for excluded volumes accompanying biological crystallization.[104] Representative of this biological strategy, polyvinylpyrrolidone, applied as a capping and crowding agent, can accelerate the growth of tellurium nanowires.[105] Since molecular crowding is generally known to influence the kinetics of self-assembly processes, its full potential as a synthetic checkpoint for NCC pathways (Figure 1) is yet to be achieved.

Of equal mechanistic importance, incorporated in the amorphous phase, stabilizing species locally accumulate solute clusters and amorphous units, restricting their dynamics, desolvation, and maturation. For instance, observed under cryogenic conditions, the ultrastructure of PILP-like phases depicts a bicontinuous organization composed of mineral species limited to about 2 nm in size, distributed in an organic matrix.[100] Interestingly, computational and experimental evidence shows the existence of a thermodynamic crossover phenomenon, wherein below a critical diameter of about 4 nm, the enhanced hydration of precrystalline cluster units yield higher stabilities relative to the anticipated crystalline phase.[106,107] Within hydrated polymer matrices, the states of hydration and structural dynamics of incorporated precrystal-

line components are distinct from those of the bulk solvent, responsible for the overall physical state and malleability of the transient phase. For instance, poly(aspartic acid) is effective at sequestering Ca^{2+} ions, forming solid precipitates at only high contents of divalent cations relative to poly(acrylic acid).[108] Attributed to hydrophilic backbone amide bonds, parallel consequences emerge for poly(aspartic acid) stabilized fluidic precursors, wherein the hydration contents of the precrystalline phase increase in proportion to the incorporated polymers.[102] In addition, delineated by organic entities, nanoscopic environments can impose certain short-range order to the occluded precrystalline units.[109] Under these conditions, the desolvation and densification of amorphous precursors, essential events for crystallization, are suppressed. For such additive-stabilized crystal precursors, an energetic penalty for expulsion of stabilizers and coassociated water molecules can limit the initiation and propagation of crystallization. Such stabilization of solvated crystal precursors can considerably lower the densities of fluidic $CaCO_3$ precursors (1.2−1.4 g/mL)[110,111] relative to solid amorphous (1.49−1.62 g/mL)[112,113] and crystalline (2.7 g/mL, calcite) counterparts, thereby enhancing the mobility and malleability of crystal precursors.

Ionic species also can control NCC via incorporation within precursors and intermediates of crystalline phases. In this mode of regulation, the ionic "dopant" modulates the physicochemical properties of precursors including the molecular composition, structural dynamics and solvation states, thereby providing exquisite control over phase transitions toward crystalline phases. For instance, analogous to PILPs, the amorphous phases of $CaCO_3$ occluding Mg^{2+} ions can yield crystalline films.[92,114] Serving as kinetic regulators of crystallization, Mg^{2+} ions enhance the degree of solvation and cohesiveness of amorphous minerals. For instance, with high contents of occluded Mg^{2+} ions, crystal precursors exhibit gel-like consistencies and hygroscopic properties.[13,115] Such interactions simultaneously invoke pronounced retardation of crystallization kinetics as well as enhanced cohesiveness of crystal precursors, factors conducive for crystallization fronts to gradually propagate through the amorphous volume, producing distinct micro- and nanocrystalline features.[13,116]

Control of NCC schemes involving amorphous precursors depends on the partitioning of additive species into three distinct functional populations (Figure 11). First, dispersed in the mother solution, additive species modulate the attachment and coalescence of precrystalline droplets and gels as well as emergent solid particles. Consequences of these interactions are often evident from the nano- and microstructure of crystalline products. For instance, in the pioneering study by Gower and Odom,[92] with increasing polymer contents, the emergent mineral crystals exhibit transitions from films toward granular particulates. The distinct evolution of crystal architectures represents mechanistic transitions from destabilization (i.e., demulsification) to depletion and electrostatic stabilization.[27,101] Second, modifying liquid/liquid and liquid/solid interfaces, adsorbents can modulate the interactions and stabilities of transient amorphous phases. For instance, macromolecules can associate with interfaces of and stabilize nanodroplets against crystallization via confinement.[97,111] Representing the third population, additives strongly associate with solute clusters forming a bicontinuous amorphous structure.[100] These species mediate the local accumulation of

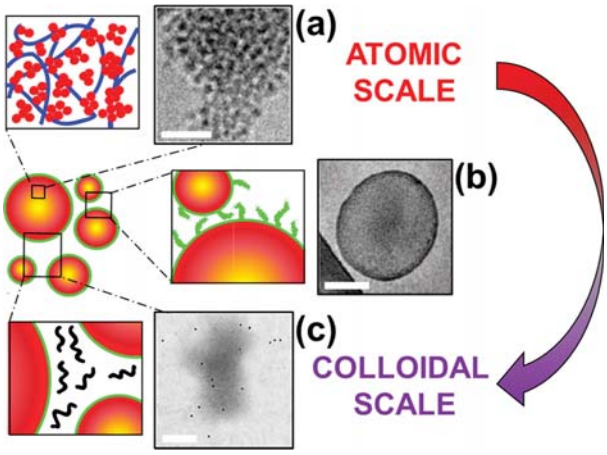

Figure 11. Modes for stabilization of amorphous precursors at distinct length scales illustrated by (a) incorporation of polymers (blue) and capping of nanoscopic clusters (red) indicated by PILP ultrastructure, (b) confinement by adsorption of additives (green) at phase interfaces illustrated by protein adsorption at interfaces of mineral nanodroplets, and (c) occupying interdroplet/particle spaces, additives (black) tune depletion (de)stabilization exemplified by spatial distribution of immunogold labeled proteins around a fluidic amorphous phase. Scale bars represent (a) 20, (b) 100, and (c) 200 nm. Adapted with permission from (a) Springer Nature, (b, c) American Chemical Society from refs 100, 101, 111.

precrystalline entities and restrict the size and dynamics of incorporated components, thereby suppressing their maturation toward thermodynamically favored states. In this mode, the overall physical state of the precrystalline phase depends on the local pH and ionic conditions, hydration states, occluded stabilizer contents, and the degree of internal cross-linking, collectively responsible for the physical state of the crystal precursor as a fluid, gel, or precipitate. In this regard, the stabilization and manipulation of amorphous precursors originates from a complex interplay encompassing the distinct functionality of stabilizer populations from atomic to colloidal scales surrounding the crystallization phenomena (Figure 11).

Directing Amorphous Phases to Complex Crystals. Approaches of NCC based on kinetically stabilized amorphous phases rely on prolonged crystallization time scales, conducive for malleable precursors to interact with local chemical environments and interfaces prior crystallization. From a simple perspective, the structural evolution of distinct forms and organizations is determined by the mechanisms of phase transformation, following solid state or dissolution reprecipitation. For a solid-state transition, the dynamics and stability of the phase boundaries of the immediate precursor determine final crystal morphologies. Here two key factors are the kinetics of transformation and "wetting" interactions with substrates. For fast transformation time scales and highly cohesive amorphous phases, solidification or crystallization occur prior to the deformation of the liquid/liquid or solid/liquid interfaces, thereby producing structures reminiscent of the precursor shape. On the other hand, for kinetically stabilized malleable precursors, the precrystalline phases can coalesce or deform and then transform. Thereby the "malleability" of kinetically stabilized amorphous precursors is harnessed toward crystallization events localized at niche interfaces and spaces of patterned or porous templates. However, bearing in mind the effective stabilization against crystallization, amor-

phous precursors accumulate high supersaturation levels and also occlude solvent (or additive) molecules occupying internal nanopores.[117] Hence the possibility of crystallization front(s) propagating through the amorphous volume via dissolution reprecipitation also presents itself.[116] In this scenario, the nature and local distribution of the stabilizer and solvent entities as well as the mobility and kinetic stability of precrystalline nanoscopic units within amorphous volumes can determine the continuity, tortuosity and spread of the crystallization front.[13]

2D and 3D templates with optimal surface chemistries effectively "mold" transiently stabilized precrystalline phases (Figure 12).[118−123] Here the interfacial interactions, cohesivity

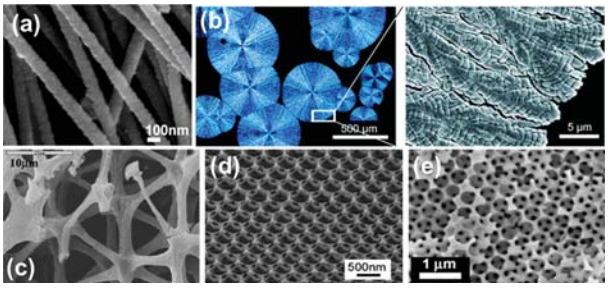

Figure 12. Complex crystal organizations derived from amorphous precursors controlled by templates such as (a) membrane pores, (b) polymer films, (c) porous hydrogels, (d, e) colloidal crystals. Reproduced with permissions from (a, b, c, e) Wiley and (d) American Chemical Society from refs 118−122.

and permeability of crystal precursors are crucial factors, tunable with the strategic application of ionic species, polymers and small organic molecules as well as optimal reaction parameters such as pH and temperature. For instance, the mineralization of organic fiber meshes is mediated by poly(aspartic acid) stabilized crystal precursors.[124] For fibers with −OH surface functionalities, the PILPs permeate the mesh structure and lead to uniform mineralization. However, with added Mg^{2+} ions, similar reactions produce spherical mineral particles, indicative of a "nonwetting" state of polymer stabilized precrystalline phases. A possible explanation lies in the incorporation of Mg^{2+} ions within amorphous precursors, which instills a hygroscopic character and maintains high cohesive forces within the amorphous precursors.[13] However, for substrates of charged nature such as peptide-decorated fibrils, an opposite trend is identified, wherein Mg^{2+} ions are essential for homogeneous PILP-mediated mineralization.[124] In this scenario, the complexation of divalent ions with substrate-immobilized amino acids (e.g., Asp, Glu, p-Ser) can render charge modulation of template surfaces. This might provide repulsive electrostatic interactions between divalent cation decorated substrates and Mg^{2+} ion and polymer costabilized amorphous phases, favoring wetting or imbibition of substrates with fluidic crystal precursors. In terms of microscopic theories for wetting behavior, the surface charge of organic scaffolds (tuned by ionic and pH conditions) emerges important in determining electrostatic contributions to the disjoining pressure. In this sense, for transient precrystalline phases, dopants and adsorbents can respectively tune the cohesivity of amorphous phases and regulate adhesive forces operating at liquid−solid or solid−solid interfaces.

During amorphous precursor mediated NCC, small organic molecules also tune the interfacial interactions between crystal precursors and template surfaces. For example, citrate molecules enhance the wettability of collagen fibrils toward poly(aspartic acid) stabilized precursors of hydroxyapatite and guide phase transformations toward nanocrystal platelets within the organic scaffold.[125,126] This mechanistic explanation is consistent with structural observations of citrate molecules localized between mineral platelets in natural bone,[127] a remnant of the formation process nonetheless functionally relevant for material mechanics. Overall, amorphous phase-mediated NCC encompasses not only the malleability and phase transitions of crystal precursors but also optimal interfacial interactions with the local chemical environments such as adsorbent-modified interfaces. Reaction parameters also serve as effective checkpoints for directing crystal morphogenesis. For example, utilizing polymer-stabilized $CaCO_3$ precursors, amorphous thin films are observed at 4 °C.[128] However, at higher temperatures (45 °C), thin films are absent due to less pronounced wetting of the substrate by amorphous phases. Instead distinct ring-like crystalline structures are produced, suggestive of limited wetting of fluidic precursors.[128] The ring-shaped crystals reflect phase transformation localized at the mineral-water interface, wherein voluminous fluidic amorphous precursors are possibly "slurped-up" by growing crystals in a sacrificial process of "core-hollowing".[110,129] Conditions of pH also influence the speciation of crystal precursors and additives, in turn affecting interactions that underlay the malleability of the precrystalline phase. For instance, polyethylenimine stabilized precursors of citrate crystals depict pH-related fluidity,[104] wherein at low pH, the speciation of citrate toward cationic forms produces an apparent loss of cohesivity.

Amorphous Precursors to Crystal Nanostructures. For diverse materials, additive-stabilized amorphous precursors often produce crystals with hierarchical nanostructures including mesocrystals.[13,130,131] With the macroscopic malleability of amorphous crystal precursors, the possibility of introducing structural hierarchy at the nanoscale is an advantage. In principle, the emergence of crystal nanostructure and crystallinity itself can be jointly determined by the spatiotemporal dynamics of phase transformation and additive localization.[132] In relation, studies demonstrate the preferential exclusion or incorporation of foreign entities such as solutes, gel networks, polymer spheres and micelles from growing crystals.[115,133−136] Similarly, even for NCC utilizing amorphous precursors, the eventual spatial distributions of molecular and ionic additives depend on properties such charge, size, rigidity, speciation, and hydration of crystallization additives, collectively determining the phase behavior of additive species toward either amorphous precursors, crystalline products or the solvent. Consider a scenario in which additives, homogeneously distributed in an amorphous volume, are gradually excluded from a propagating crystallization front and enriched in the diminishing amorphous volume. This can occur due to an inability to incorporate within the host crystal lattice, resulting in discontinuous crystallization fronts that produce pockets or layers of additive-enriched amorphous material resistant toward crystallization. In nature, these amorphous residues of phase transformation are efficiently utilized to introduce structural hierarchy in emergent organizations.[11,137] Further, in case that the extruded additives exhibit crystal face-specific adsorption, emergent

nanocrystals are stabilized against further growth despite engulfed by amorphous precursors. For such conditions, the amorphous byproducts occupying intercrystalline spaces can serve as a viscoelastic medium for OA phenomena involving the crystalline nanoparticles.

For amorphous precursor based NCC pathways, crystallization kinetics and volume continuity of amorphous precursors are important determinants of crystal architecture (Figure 13). This is demonstrated for the controlled

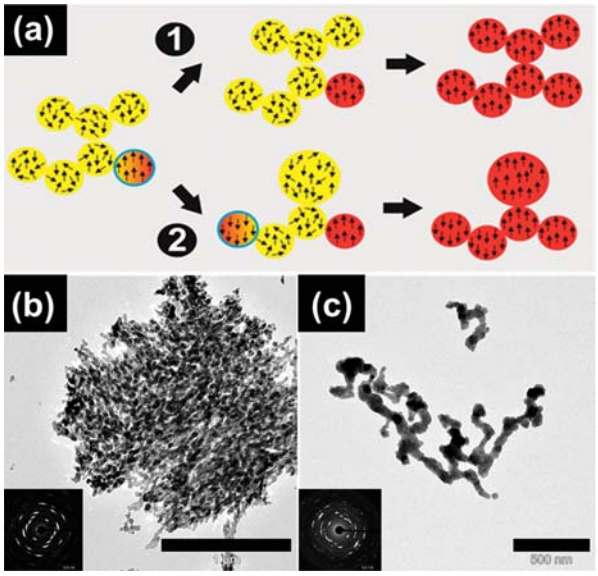

Figure 13. (a) Representation of amorphous (yellow) to crystalline (red) transformation at (1) slow rates enabling gradual propagation of a reaction boundary and nanocrystal coalignment and (2) rapid rates producing multiple crystal nucleation sites and crystallographic misalignment. This is exemplified by crystallographic continuity in precursor volumes at larger length scales during (b) gradual transformation relative to (c) faster reaction rates. Adapted from ref 13 with permission of Royal Society of Chemistry.

crystallization of amorphous precursors in defined water environments.[13] For slow crystallization of amorphous precursors, the gradual release of "impurities" and solvent molecules enable time scale conducive for OA or fusion of nanocrystals. On the other hand, rapid crystallization produces multiple nucleation sites distributing the amorphous volume into smaller, disoriented crystal domains. In addition, the cohesiveness of amorphous precursors as well as the possible extrusion of the dopant species during nanocrystal formation can result in compact, well-organized nano- or microstructures such as mesocrystals.[13] Hence the kinetics of phase transformation can critically determine the spatial propagation of crystallization fronts toward defined superstructures.

By deconstructing the crystallization process into two steps, bioinspired "disordered by design" amorphous precursors can significantly expand synthetic strategies toward functional materials. For instance, by temperature regulation and solvent engineering, the transient stabilization and transformation of amorphous intermediates enable the growth of $CH_3NH_3PbBr_3$ crystals with a preferential [001] orientation and smooth finishing on porous scaffolds.[138] Exhibiting augmented performance and stability, this hybrid organic/inorganic perovskite material exemplifies the technological scope of amorphous precursors toward high quality functional crystals via NCC. Harnessing amorphous precursors, a two-step hydrothermal approach realized brookite TiO_2 mesocrystals.[139] By using amorphous titanate precursors and oxalic acid as a structure-directing additive, the resultant crystals exhibit mesocrystalline domains and demonstrate impressive electrochemical performance as the anode in lithium-ion batteries. Assembled with nanocrystal subunits, the mesocrystalline anode is suggested to enhance contact with the electrolyte, thereby facilitating electron and ion transport processes. Analogous to biomineralization mechanisms, amorphous phases can also be applied as a multifunctional matrix for nanocrystal growth, which concomitantly inhibits the growth and fusion of nascent crystals. This is exemplified by a microwave-assisted nonaqueous sol−gel method in which Nb:TiO_2 subunits grow and assemble in a mutual crystallographic direction within an amorphous Sb-rich medium.[140] Relative to single crystals, the superstructured material shows enhanced photocatalytic activity, attributed to higher porosity and reactivity of mesocrystals. In this manner, amorphous precursor based NCC can effectively direct the growth and structure of complex crystalline structures with superior functional properties.

Relative to nanocrystal-mediated NCC, the mechanistic details of amorphous precursor mediated NCC are less clear. However, few studies address the connection between the spatiotemporal dynamics of additives and phase transformation of amorphous precursors. For certain polymer-stabilized amorphous precursors, the polymer units distributed in the nanostructure stabilize precrystalline nanoclusters.[100] However, on crystallization, the emergent crystals are often enveloped by a polymer film, indicative of the high mobility of additives within the amorphous volume and also their active exclusion during crystallization.[141,142] Additive species can also be excluded during amorphous-to-amorphous transitions. For instance, the release of charged molecules from amorphous droplets triggers the formation of hollow amorphous particles via a "core-hollowing" transformation.[110] Under special circumstances, entities excluded from the amorphous phase can produce a secondary phase that occupies intracrystalline spaces as nanofilms, enabling oriented assembly or growth however hindering fusion of nascent nanocrystals.[13] As exemplified by biogenic crystals,[11] these additive-controlled transformation reactions can inspire synthetic avenues to achieve precise coalignment of nanocrystals at supermicrometer length scales. For example, SM50 proteins, abundant in sea urchins, stabilize amorphous calcium carbonate nanoparticles within vesicles in a similar way to the growth of natural sea urchin spicules. Enzymatic cleavage of this protein producing a C-type lectin domain (CTL domain) led to mesocrystal formation,[111] which is the structure of the natural sea urchin spine.[11] This demonstrates the tremendous potential of additive engineering in order to control NCC pathways in space and time. Given the multistep and multicomponent nature of NCC schemes, the rational design of additives to selectively associate with or exclude from ion and ion-clusters, liquid condensed phases, amorphous precursors as well as crystalline products represents a powerful means to achieve synthetic control over the kinetics and structural outcomes of crystallization.

CONCLUSION AND OUTLOOK

The examples discussed above demonstrate the capabilities of crystallization via NCC pathways in an impressive manner. Although OA was discovered already 20 years ago and also mesocrystals have been known for more than a decade, the exact mechanisms of mesocrystal formation or OA could only be partially revealed. This results from the significant analytical challenges for in situ analysis in solution. Fortunately, in situ AFM and LC-TEM techniques enabled the observation of elementary steps in mesocrystal formation and OA. OA is the NCC mechanism, which is so far known best and has been experimentally well documented so that the contributing forces and mechanistic details are known and predictions start to become possible. For mesocrystals, the research is less mature, although the formation mechanisms of several mesocrystal systems could be revealed. However, up to now, already 7 different formation mechanisms of mesocrystals are known and there are likely more. This makes clear that there is not only a single pathway toward mesocrystals like the oriented aggregation of nanocrystals as shown in Figure 1c, but there are also more as summarized in other overviews.[38,39] This requires different analytical approaches toward revealing the formation mechanisms of mesocrystals and is a reason why, so far, no theoretical approach exists to describe the formation of mesocrystals. Therefore, the research on mesocrystals still remains partly empirical. Nevertheless, the superior physical and chemical properties of mesocrystals show their huge potential in several important areas like electrode materials, catalysts, storage materials, or building materials, and this will initiate further intense research toward a mechanistic understanding.

The observation and analysis of cluster and liquid precursor pathways remains, however, much more challenging as these species are not visible in in situ AFM or HRTEM, and cryoTEM investigations have their own challenges. In addition, the multistep nature of these NCC pathways involving species with sizes from around a nanometer to several micrometers and involving (nano)phase separation makes their observation notoriously difficult. A good example is the prenucleation cluster pathway,[5,91] which is so far only revealed for very few systems.

Despite the analytical challenges to reveal the NCC mechanisms and the general lack of a theory for NCC, the potential is obvious since the big advantage of these multistep crystallization pathways is the possibility to influence the mechanism at each elementary step by change of the reaction conditions or additives. Further mechanistic knowledge will greatly enhance these possibilities and open new horizons for NCC toward the synthesis of advanced materials to address present and future challenges of society.

AUTHOR INFORMATION

Corresponding Authors

*marie.jehannin@uni-konstanz.de
*a.r.rao@utwente.nl
*helmut.coelfen@uni-konstanz.de

ORCID

Marie Jehannin: 0000-0002-1770-6240
Helmut Cölfen: 0000-0002-1148-0308

Author Contributions

‖M.J., A.R., and H.C. contributed equally.

Notes

The authors declare no competing financial interest.

ACKNOWLEDGMENTS

M.J. and H.C. thank the Deutsche Forschungsgemeinschaft (DFG) for funding their research on Mesocrystals and Nonclassical Crystallization via projects CO194/19-1 (M.J. and H.C.) 194/16-1 and 194/21-1 (H.C.), and SFB 1214 projects B1 and B3 (H.C.).

REFERENCES

(1) Cölfen, H.; Antonietti, M. *Mesocrystals and Nonclassical Crystallization*; John Wiley & Sons: Chichester, 2008.

(2) De Yoreo, J. J.; Gilbert, P.; Sommerdijk, N.; Penn, R. L.; Whitelam, S.; Joester, D.; Zhang, H. Z.; Rimer, J. D.; Navrotsky, A.; Banfield, J. F.; Wallace, A. F.; Michel, F. M.; Meldrum, F. C.; Colfen, H.; Dove, P. M. Crystallization by particle attachment in synthetic, biogenic, and geologic environments. *Science* **2015**, *349* (6247), aaa6760.

(3) Wolf, S. E.; Bohm, C. F.; Harris, J.; Demmert, B.; Jacob, D. E.; Mondeshki, M.; Ruiz-Agudo, E.; Rodriguez-Navarro, C. Nonclassical crystallization in vivo et in vitro (I): Process-structure-property relationships of nanogranular biominerals. *J. Struct. Biol.* **2016**, *196* (2), 244−259.

(4) Rodriguez-Navarro, C.; Ruiz-Agudo, E.; Harris, J.; Wolf, S. E. Nonclassical crystallization in vivo et in vitro (II): Nanogranular features in biomimetic minerals disclose a general colloid-mediated crystal growth mechanism. *J. Struct. Biol.* **2016**, *196* (2), 260−287.

(5) Gebauer, D.; Wolf, S. E. Thinking solid materials from their solute state: a shift in paradigms towards a holistic approach in functional materials chemistry. *J. Am. Chem. Soc.* **2019**, *141* (11), 4490−4505.

(6) Niederberger, M.; Colfen, H. Oriented attachment and mesocrystals: Non-classical crystallization mechanisms based on nanoparticle assembly. *Phys. Chem. Chem. Phys.* **2006**, *8* (28), 3271−3287.

(7) Yuwono, V. M.; Burrows, N. D.; Soltis, J. A.; Penn, R. L. Oriented Aggregation: Formation and Transformation of Mesocrystal Intermediates Revealed. *J. Am. Chem. Soc.* **2010**, *132* (7), 2163.

(8) Schwahn, D.; Ma, Y. R.; Colfen, H. Mesocrystal to single crystal transformation of D,L-alanine evidenced by small angle neutron scattering. *J. Phys. Chem. C* **2007**, *111* (8), 3224−3227.

(9) Li, D.; Nielsen, M. H.; Lee, J. R. I.; Frandsen, C.; Banfield, J. F.; De Yoreo, J. J. Direction-Specific Interactions Control Crystal Growth by Oriented Attachment. *Science* **2012**, *336* (6084), 1014−1018.

(10) Politi, Y.; Metzler, R. A.; Abrecht, M.; Gilbert, B.; Wilt, F. H.; Sagi, I.; Addadi, L.; Weiner, S.; Gilbert, P. Transformation mechanism of amorphous calcium carbonate into calcite in the sea urchin larval spicule. *Proc. Natl. Acad. Sci. U. S. A.* **2008**, *105* (45), 17362−17366.

(11) Seto, J.; Ma, Y. R.; Davis, S. A.; Meldrum, F.; Gourrier, A.; Kim, Y. Y.; Schilde, U.; Sztucki, M.; Burghammer, M.; Maltsev, S.; Jager, C.; Colfen, H. Structure-property relationships of a biological mesocrystal in the adult sea urchin spine. *Proc. Natl. Acad. Sci. U. S. A.* **2012**, *109* (10), 3699−3704.

(12) Yu, P. T.; Tsao, C.; Wang, C. C.; Chang, C. Y.; Wang, C. H.; Chan, J. C. C. High-Magnesium Calcite Mesocrystals: Formation in Aqueous Solution under Ambient Conditions. *Angew. Chem., Int. Ed.* **2017**, *56* (51), 16202−16206.

(13) Huang, Y. C.; Gindele, M. B.; Knaus, J.; Rao, A.; Gebauer, D. On mechanisms of mesocrystal formation: magnesium ions and water environments regulate the crystallization of amorphous minerals. *CrystEngComm* **2018**, *20* (31), 4395.

(14) Rao, A.; Cölfen, H. From Solute, Fluidic and Particulate Precursors to Complex Organizations of Matter. *Chem. Rec.* **2018**, *18* (7−8), 1203−1221.

(15) Liu, J.; Shen, T.; Yang, Z. H.; Zhang, S.; Sun, G. Y. Multistep Heterogeneous Nucleation in Binary Mixtures of Charged Colloidal Spheres. *J. Phys. Chem. Lett.* **2017**, *8* (19), 4652−4658.

(16) Kawasaki, T.; Tanaka, H. Formation of a crystal nucleus from liquid. *Proc. Natl. Acad. Sci. U. S. A.* **2010**, *107* (32), 14036−14041.
(17) Peng, Y.; Wang, F.; Wang, Z.; Alsayed, A. M.; Zhang, Z.; Yodh, A. G.; Han, Y. Two-step nucleation mechanism in solid−solid phase transitions. *Nat. Mater.* **2015**, *14* (1), 101.
(18) Gasser, U.; Weeks, E. R.; Schofield, A.; Pusey, P.; Weitz, D. Real-space imaging of nucleation and growth in colloidal crystallization. *Science* **2001**, *292* (5515), 258−262.
(19) Jacobson, L. C.; Hujo, W.; Molinero, V. Amorphous precursors in the nucleation of clathrate hydrates. *J. Am. Chem. Soc.* **2010**, *132* (33), 11806−11811.
(20) Lupi, L.; Hudait, A.; Peters, B.; Grünwald, M.; Mullen, R. G.; Nguyen, A. H.; Molinero, V. Role of stacking disorder in ice nucleation. *Nature* **2017**, *551* (7679), 218.
(21) Loh, N. D.; Sen, S.; Bosman, M.; Tan, S. F.; Zhong, J.; Nijhuis, C. A.; Král, P.; Matsudaira, P.; Mirsaidov, U. Multistep nucleation of nanocrystals in aqueous solution. *Nat. Chem.* **2017**, *9* (1), 77.
(22) Ishizuka, S.; Kimura, Y.; Yamazaki, T.; Hama, T.; Watanabe, N.; Kouchi, A. Two-step process in homogeneous nucleation of alumina in supersaturated vapor. *Chem. Mater.* **2016**, *28* (23), 8732−8741.
(23) Bewernitz, M. A.; Gebauer, D.; Long, J.; Cölfen, H.; Gower, L. B. A metastable liquid precursor phase of calcium carbonate and its interactions with polyaspartate. *Faraday Discuss.* **2012**, *159* (1), 291−312.
(24) Gebauer, D.; Völkel, A.; Cölfen, H. Stable prenucleation calcium carbonate clusters. *Science* **2008**, *322* (5909), 1819−1822.
(25) Sebastiani, F.; Wolf, S. L.; Born, B.; Luong, T. Q.; Cölfen, H.; Gebauer, D.; Havenith, M. Water dynamics from THz spectroscopy reveal the locus of a liquid−liquid binodal limit in aqueous CaCO3 solutions. *Angew. Chem., Int. Ed.* **2017**, *56* (2), 490−495.
(26) Wallace, A. F.; Hedges, L. O.; Fernandez-Martinez, A.; Raiteri, P.; Gale, J. D.; Waychunas, G. A.; Whitelam, S.; Banfield, J. F.; De Yoreo, J. J. Microscopic evidence for liquid-liquid separation in supersaturated CaCO3 solutions. *Science* **2013**, *341* (6148), 885−889.
(27) Wolf, S. E.; Gower, L. B. Challenges and perspectives of the polymer-induced liquid-precursor process: the pathway from liquid-condensed mineral precursors to mesocrystalline products. In *New Perspectives on Mineral Nucleation and Growth*; Springer: 2017; pp 43−75.
(28) Rodriguez-Navarro, C.; Burgos Cara, A.; Elert, K.; Putnis, C. V.; Ruiz-Agudo, E. Direct nanoscale imaging reveals the growth of calcite crystals via amorphous nanoparticles. *Cryst. Growth Des.* **2016**, *16* (4), 1850−1860.
(29) Schreiber, R. E.; Houben, L.; Wolf, S. G.; Leitus, G.; Lang, Z.-L.; Carbó, J. J.; Poblet, J. M.; Neumann, R. Real-time molecular scale observation of crystal formation. *Nat. Chem.* **2017**, *9* (4), 369.
(30) Lupulescu, A. I.; Rimer, J. D. In situ imaging of silicalite-1 surface growth reveals the mechanism of crystallization. *Science* **2014**, *344* (6185), 729−732.
(31) Schubert, R.; Meyer, A.; Baitan, D.; Dierks, K.; Perbandt, M.; Betzel, C. Real-time observation of protein dense liquid cluster evolution during nucleation in protein crystallization. *Cryst. Growth Des.* **2017**, *17* (3), 954−958.
(32) Yamazaki, T.; Kimura, Y.; Vekilov, P. G.; Furukawa, E.; Shirai, M.; Matsumoto, H.; Van Driessche, A. E.; Tsukamoto, K. Two types of amorphous protein particles facilitate crystal nucleation. *Proc. Natl. Acad. Sci. U. S. A.* **2017**, *114* (9), 2154−2159.
(33) Vivarès, D.; Kaler, E. W.; Lenhoff, A. M. Quantitative imaging by confocal scanning fluorescence microscopy of protein crystallization via liquid−liquid phase separation. *Acta Crystallogr., Sect. D: Biol. Crystallogr.* **2005**, *61* (6), 819−825.
(34) Jiang, Y.; Kellermeier, M.; Gebauer, D.; Lu, Z.; Rosenberg, R.; Moise, A.; Przybylski, M.; Cölfen, H. Growth of organic crystals via attachment and transformation of nanoscopic precursors. *Nat. Commun.* **2017**, *8*, 15933.
(35) Ni, B.; He, T.; Wang, J. O.; Zhang, S. M.; Ouyang, C.; Long, Y.; Zhuang, J.; Wang, X. The formation of (NiFe)S-2 pyrite mesocrystals as efficient pre-catalysts for water oxidation. *Chemical Science* **2018**, *9* (10), 2762−2767.
(36) Tsarfati, Y.; Rosenne, S.; Weissman, H.; Shimon, L. J. W.; Gur, D.; Palmer, B. A.; Rybtchinski, B. Crystallization of Organic Molecules: Nonclassical Mechanism Revealed by Direct Imaging. *ACS Cent. Sci.* **2018**, *4* (8), 1031−1036.
(37) Meldrum, F. C.; Colfen, H. Controlling Mineral Morphologies and Structures in Biological and Synthetic Systems. *Chem. Rev.* **2008**, *108* (11), 4332−4432.
(38) Sturm, E. V.; Colfen, H. Mesocrystals: Past, Presence, Future. *Crystals* **2017**, *7* (7), 207.
(39) Sturm, E. V.; Colfen, H. Mesocrystals: structural and morphogenetic aspects. *Chem. Soc. Rev.* **2016**, *45* (21), 5821−5833.
(40) Colfen, H.; Antonietti, M. Mesocrystals: Inorganic superstructures made by highly parallel crystallization and controlled alignment. *Angew. Chem., Int. Ed.* **2005**, *44* (35), 5576−5591.
(41) Zhang, P.; Tachikawa, T.; Fujitsuka, M.; Majima, T. The Development of Functional Mesocrystals for Energy Harvesting, Storage, and Conversion. *Chem. - Eur. J.* **2018**, *24* (24), 6295.
(42) Uchaker, E.; Cao, G. Z. Mesocrystals as electrode materials for lithium-ion batteries. *Nano Today* **2014**, *9* (4), 499−524.
(43) Tachikawa, T.; Majima, T. Metal oxide mesocrystals with tailored structures and properties for energy conversion and storage applications. *NPG Asia Mater.* **2014**, *6*, e100.
(44) Ma, M. G.; Colfen, H. Mesocrystals - Applications and potential. *Curr. Opin. Colloid Interface Sci.* **2014**, *19* (2), 56−65.
(45) Wu, H. L.; Yang, Y. K.; Ou, Y.; Lu, B.; Li, J.; Yuan, W. T.; Wang, Y.; Zhang, Z. Early Stage Growth of Rutile Titania Mesocrystals. *Cryst. Growth Des.* **2018**, *18* (8), 4209−4214.
(46) Brunner, J.; Baburin, I. A.; Sturm, S.; Kvashnina, K.; Rossberg, A.; Pietsch, T.; Andreev, S.; Sturm, E.; Colfen, H. Self-Assembled Magnetite Mesocrystalline Films: Toward Structural Evolution from 2D to 3D Superlattices. *Adv. Mater. Interfaces* **2017**, *4* (1), 1600431.
(47) Wetterskog, E.; Klapper, A.; Disch, S.; Josten, E.; Hermann, R. P.; Rucker, U.; Bruckel, T.; Bergstrom, L.; Salazar-Alvarez, G. Tuning the structure and habit of iron oxide mesocrystals. *Nanoscale* **2016**, *8* (34), 15571−15580.
(48) Agthe, M.; Plivelic, T. S.; Labrador, A.; Bergstrom, L.; Salazar-Alvarez, G. Following in Real Time the Two-Step Assembly of Nanoparticles into Mesocrystals in Levitating Drops. *Nano Lett.* **2016**, *16* (11), 6838−6843.
(49) Kapuscinski, M.; Agthe, M.; Bergstrom, L. Time-resolved viscoelastic properties of self-assembling iron oxide nanocube superlattices probed by quartz crystal microbalance with dissipation monitoring. *J. Colloid Interface Sci.* **2018**, *522*, 104−110.
(50) Zaluzhnvy, I. A.; Kurta, R. P.; Andre, A.; Gorobtsov, O. Y.; Rose, M.; Skopintsev, P.; Besedin, I.; Zozulya, A. V.; Sprung, M.; Schreiber, F.; Vartanyants, I. A.; Scheele, M. Quantifying Angular Correlations between the Atomic Lattice and the Superlattice of Nanocrystals Assembled with Directional Linking. *Nano Lett.* **2017**, *17* (6), 3511−3517.
(51) Wang, L.; Cai, M. J.; Sun, W.; He, L.; Zhang, X. H. Promoting Charge Separation in Semiconductor Nanocrystal Superstructures for Enhanced Photocatalytic Activity. *Adv. Mater. Interfaces* **2018**, *5* (13), 1701694.
(52) Li, C. C.; Yin, X. M.; Li, Q. H.; Wang, T. H. Enhanced gas sensing properties of ZnO/SnO2 hierarchical architectures by glucose-induced attachment. *CrystEngComm* **2011**, *13* (5), 1557−1563.
(53) Zhong, P.; Liu, H. P.; Zhang, J.; Yin, Y. D.; Gao, C. B. Controlled Synthesis of Octahedral Platinum-Based Mesocrystals by Oriented Aggregation. *Chem. - Eur. J.* **2017**, *23* (28), 6803−6810.
(54) Tan, B. Y.; Ye, X. Z.; Li, Y. J.; Ma, X. Q.; Wang, Y.; Ye, J. F. Defective Anatase TiO2-x Mesocrystal Growth In Situ on g-C3N4 Nanosheets: Construction of 3D/2D Z-Scheme Heterostructures for Highly Efficient Visible-Light Photocatalysis. *Chem. - Eur. J.* **2018**, *24* (50), 13311−13321.
(55) Ding, Z. P.; Zhang, D. T.; Feng, Y. M.; Zhang, F.; Chen, L. B.; Du, Y.; Ivey, D. G.; Wei, W. F. Tuning anisotropic ion transport in

mesocrystalline lithium orthosilicate nanostructures with preferentially exposed facets. *NPG Asia Mater.* **2018**, *10*, 606.
(56) Mao, L. B.; Gao, H. L.; Yao, H. B.; Liu, L.; Colfen, H.; Liu, G.; Chen, S. M.; Li, S. K.; Yan, Y. X.; Liu, Y. Y.; Yu, S. H. Synthetic nacre by predesigned matrix-directed mineralization. *Science* **2016**, *354* (6308), 107−110.
(57) Picker, A.; Nicoleau, L.; Burghard, Z.; Bill, J.; Zlotnikov, I.; Labbez, C.; Nonat, A.; Colfen, H. Mesocrystalline calcium silicate hydrate: A bioinspired route toward elastic concrete materials. *Sci. Adv.* **2017**, *3* (11), e1701216.
(58) Picker, A.; Nicoleau, L.; Nonat, A.; Labbez, C.; Colfen, H. Identification of Binding Peptides on Calcium Silicate Hydrate: A Novel View on Cement Additives. *Adv. Mater.* **2014**, *26* (7), 1135−1140.
(59) Hwang, J.; Heil, T.; Antonietti, M.; Schmidt, B. Morphogenesis of Metal-Organic Mesocrystals Mediated by Double Hydrophilic Block Copolymers. *J. Am. Chem. Soc.* **2018**, *140* (8), 2947−2956.
(60) Tao, F.; Han, Q.; Liu, K. Q.; Yang, P. Tuning Crystallization Pathways through the Mesoscale Assembly of Biomacromolecular Nanocrystals. *Angew. Chem., Int. Ed.* **2017**, *56* (43), 13440−13444.
(61) Li, G. L.; Ma, P.; He, Y.; Zhang, Y. F.; Luo, Y. N.; Zhang, C.; Fan, H. M. Enzyme-Nanowire Mesocrystal Hybrid Materials with an Extremely High Biocatalytic Activity. *Nano Lett.* **2018**, *18* (9), 5919−5926.
(62) Matsumoto, R.; Yamazaki, H.; Takasaki, M.; Oaki, Y.; Sato, T.; Imai, H. Nanoscale Mosaic Works: Tetragonal Lattices of Iso-Oriented Heterogeneous Nanocubes. *Langmuir* **2018**, *34* (13), 4031−4035.
(63) Simon, P.; Bahrig, L.; Baburin, I. A.; Formanek, P.; Roder, F.; Sickmann, J.; Hickey, S. G.; Eychmuller, A.; Lichte, H.; Kniep, R.; Rosseeva, E. Interconnection of Nanoparticles within 2D Superlattices of PbS/Oleic Acid Thin Films. *Adv. Mater.* **2014**, *26* (19), 3042−3049.
(64) Xue, J. W.; Elbanna, O.; Kim, S.; Fujitsuka, M.; Majima, T. Defect state-induced efficient hot electron transfer in Au nanoparticles/reduced TiO2 mesocrystal photocatalysts. *Chem. Commun.* **2018**, *54* (47), 6052−6055.
(65) Elbanna, O.; Kim, S.; Fujitsuka, M.; Majima, T. TiO2 mesocrystals composited with gold nanorods for highly efficient visible-NIR-photocatalytic hydrogen production. *Nano Energy* **2017**, *35*, 1−8.
(66) Penn, R. L.; Banfield Jillian, F. Oriented attachment and growth, twinning, polytypism, and formation of metastable phases: Insights from nanocrystalline TiO2. *Am. Mineral.* **1998**, *83*, 1077.
(67) Penn, R. L.; Banfield, J. F. Imperfect Oriented Attachment: Dislocation Generation in Defect-Free Nanocrystals. *Science* **1998**, *281* (5379), 969−971.
(68) Nakouzi, E.; Soltis, J. A.; Legg, B. A.; Schenter, G. K.; Zhang, X.; Graham, T. R.; Rosso, K. M.; Anovitz, L. M.; De Yoreo, J. J.; Chun, J. Impact of Solution Chemistry and Particle Anisotropy on the Collective Dynamics of Oriented Aggregation. *ACS Nano* **2018**, *12* (10), 10114−10122.
(69) Zhang, H.; Banfield, J. F. Energy Calculations Predict Nanoparticle Attachment Orientations and Asymmetric Crystal Formation. *J. Phys. Chem. Lett.* **2012**, *3* (19), 2882−2886.
(70) Zhu, C.; Liang, S.; Song, E.; Zhou, Y.; Wang, W.; Shan, F.; Shi, Y.; Hao, C.; Yin, K.; Zhang, T.; Liu, J.; Zheng, H.; Sun, L. In-situ liquid cell transmission electron microscopy investigation on oriented attachment of gold nanoparticles. *Nat. Commun.* **2018**, *9* (1), 421.
(71) Banfield, J. F.; Welch, S. A.; Zhang, H.; Ebert, T. T.; Penn, R. L. Aggregation-Based Crystal Growth and Microstructure Development in Natural Iron Oxyhydroxide Biomineralization Products. *Science* **2000**, *289* (5480), 751−754.
(72) Killian, C. E.; Metzler, R. A.; Gong, Y. U. T.; Olson, I. C.; Aizenberg, J.; Politi, Y.; Wilt, F. H.; Scholl, A.; Young, A.; Doran, A.; Kunz, M.; Tamura, N.; Coppersmith, S. N.; Gilbert, P. U. P. A. Mechanism of Calcite Co-Orientation in the Sea Urchin Tooth. *J. Am. Chem. Soc.* **2009**, *131* (51), 18404−18409.
(73) Ondry, J. C.; Hauwiller, M. R.; Alivisatos, A. P. Dynamics and Removal Pathway of Edge Dislocations in Imperfectly Attached PbTe Nanocrystal Pairs: Toward Design Rules for Oriented Attachment. *ACS Nano* **2018**, *12* (4), 3178−3189.
(74) Xue, X.; Penn, R. L.; Leite, E. R.; Huang, F.; Lin, Z. Crystal growth by oriented attachment: kinetic models and control factors. *CrystEngComm* **2014**, *16* (8), 1419−1429.
(75) Schliehe, C.; Juarez, B. H.; Pelletier, M.; Jander, S.; Greshnykh, D.; Nagel, M.; Meyer, A.; Foerster, S.; Kornowski, A.; Klinke, C.; Weller, H. Ultrathin PbS Sheets by Two-Dimensional Oriented Attachment. *Science* **2010**, *329* (5991), 550−553.
(76) Cho, K.-S.; Talapin, D. V.; Gaschler, W.; Murray, C. B. Designing PbSe Nanowires and Nanorings through Oriented Attachment of Nanoparticles. *J. Am. Chem. Soc.* **2005**, *127* (19), 7140−7147.
(77) Tan Shu, F.; Raj, S.; Bisht, G.; Annadata Harshini, V.; Nijhuis Christian, A.; Král, P.; Mirsaidov, U. Nanoparticle Interactions Guided by Shape-Dependent Hydrophobic Forces. *Adv. Mater.* **2018**, *30* (16), 1707077.
(78) Liao, H.-G.; Cui, L.; Whitelam, S.; Zheng, H. Real-Time Imaging of Pt3Fe Nanorod Growth in Solution. *Science* **2012**, *336* (6084), 1011−1014.
(79) Liu, Z.; Pan, H.; Zhu, G.; Li, Y.; Tao, J.; Jin, B.; Tang, R. Realignment of Nanocrystal Aggregates into Single Crystals as a Result of Inherent Surface Stress. *Angew. Chem., Int. Ed.* **2016**, *55* (41), 12836−12840.
(80) Zhang, H.; Banfield, J. F. Interatomic Coulombic interactions as the driving force for oriented attachment. *CrystEngComm* **2014**, *16* (8), 1568−1578.
(81) Zhang, X.; Shen, Z.; Liu, J.; Kerisit, S. N.; Bowden, M. E.; Sushko, M. L.; De Yoreo, J. J.; Rosso, K. M. Direction-specific interaction forces underlying zinc oxide crystal growth by oriented attachment. *Nat. Commun.* **2017**, *8* (1), 835.
(82) Zhang, X.; He, Y.; Sushko, M. L.; Liu, J.; Luo, L.; De Yoreo, J. J.; Mao, S. X.; Wang, C.; Rosso, K. M. Direction-specific van der Waals attraction between rutile TiO_2 nanocrystals. *Science* **2017**, *356* (6336), 434−437.
(83) Kim, D. H.; Park, J.; Li, Z.; Yang, M.; Park, J.-S.; Park, I. J.; Kim, J. Y.; Berry, J. J.; Rumbles, G.; Zhu, K. 300% Enhancement of Carrier Mobility in Uniaxial-Oriented Perovskite Films Formed by Topotactic-Oriented Attachment. *Adv. Mater.* **2017**, *29* (23), 1606831.
(84) Liang, Y.; Li, Y.; Wang, H.; Zhou, J.; Wang, J.; Regier, T.; Dai, H. Co3O4 nanocrystals on graphene as a synergistic catalyst for oxygen reduction reaction. *Nat. Mater.* **2011**, *10*, 780.
(85) Li, M.; Zhao, Z.; Cheng, T.; Fortunelli, A.; Chen, C.-Y.; Yu, R.; Zhang, Q.; Gu, L.; Merinov, B. V.; Lin, Z.; Zhu, E.; Yu, T.; Jia, Q.; Guo, J.; Zhang, L.; Goddard, W. A.; Huang, Y.; Duan, X. Ultrafine jagged platinum nanowires enable ultrahigh mass activity for the oxygen reduction reaction. *Science* **2016**, *354* (6318), 1414−1419.
(86) Ma, Y.; Gao, W.; Shan, H.; Chen, W.; Shang, W.; Tao, P.; Song, C.; Addiego, C.; Deng, T.; Pan, X.; Wu, J. Platinum-Based Nanowires as Active Catalysts toward Oxygen Reduction Reaction: In Situ Observation of Surface-Diffusion-Assisted. *Adv. Mater.* **2017**, *29* (46), 1703460.
(87) Tétreault, N.; Horváth, E.; Moehl, T.; Brillet, J.; Smajda, R.; Bungener, S.; Cai, N.; Wang, P.; Zakeeruddin, S. M.; Forró, L.; Magrez, A.; Grätzel, M. High-Efficiency Solid-State Dye-Sensitized Solar Cells: Fast Charge Extraction through Self-Assembled 3D Fibrous Network of Crystalline TiO2 Nanowires. *ACS Nano* **2010**, *4* (12), 7644−7650.
(88) Wang, C.; Zhou, Y.; Ge, M.; Xu, X.; Zhang, Z.; Jiang, J. Z. Large-Scale Synthesis of SnO2 Nanosheets with High Lithium Storage Capacity. *J. Am. Chem. Soc.* **2010**, *132* (1), 46−47.
(89) Wang, C.; Du, G.; Ståhl, K.; Huang, H.; Zhong, Y.; Jiang, J. Z. Ultrathin SnO2 Nanosheets: Oriented Attachment Mechanism, Nonstoichiometric Defects, and Enhanced Lithium-Ion Battery Performances. *J. Phys. Chem. C* **2012**, *116* (6), 4000−4011.

(90) Chen, X.; Zhou, Y.; Liu, Q.; Li, Z.; Liu, J.; Zou, Z. Ultrathin, Single-Crystal WO3 Nanosheets by Two-Dimensional Oriented Attachment toward Enhanced Photocatalystic Reduction of CO2 into Hydrocarbon Fuels under Visible Light. *ACS Appl. Mater. Interfaces* **2012**, *4* (7), 3372−3377.
(91) Gebauer, D.; Kellermeier, M.; Gale, J. D.; Bergström, L.; Cölfen, H. Pre-nucleation clusters as solute precursors in crystallisation. *Chem. Soc. Rev.* **2014**, *43* (7), 2348−2371.
(92) Gower, L. B.; Odom, D. J. Deposition of calcium carbonate films by a polymer-induced liquid-precursor (PILP) process. *J. Cryst. Growth* **2000**, *210* (4), 719−734.
(93) Wolf, S. L.; Caballero, L.; Melo, F.; Cölfen, H. Gel-like calcium carbonate precursors observed by in situ AFM. *Langmuir* **2017**, *33* (1), 158−163.
(94) Galkin, O.; Vekilov, P. G. Control of protein crystal nucleation around the metastable liquid−liquid phase boundary. *Proc. Natl. Acad. Sci. U. S. A.* **2000**, *97* (12), 6277−6281.
(95) Rao, A.; Cölfen, H. From Solute, Fluidic and Particulate Precursors to Complex Organizations of Matter. *Chem. Rec.* **2018**, *18*, 1203.
(96) Navrotsky, A. Energetic clues to pathways to biomineralization: Precursors, clusters, and nanoparticles. *Proc. Natl. Acad. Sci. U. S. A.* **2004**, *101* (33), 12096−12101.
(97) Rao, A.; Drechsler, M.; Schiller, S.; Scheffner, M.; Gebauer, D.; Cölfen, H. Stabilization of Mineral Precursors by Intrinsically Disordered Proteins. *Adv. Funct. Mater.* **2018**, *28* (37), 1802063.
(98) Sun, S.; Gebauer, D.; Cölfen, H. A general strategy for colloidal stable ultrasmall amorphous mineral clusters in organic solvents. *Chemical science* **2017**, *8* (2), 1400−1405.
(99) Gebauer, D.; Cölfen, H.; Verch, A.; Antonietti, M. The multiple roles of additives in CaCO3 crystallization: A quantitative case study. *Adv. Mater.* **2009**, *21* (4), 435−439.
(100) Xu, Y.; Tijssen, K. C.; Bomans, P. H.; Akiva, A.; Friedrich, H.; Kentgens, A. P.; Sommerdijk, N. A. Microscopic structure of the polymer-induced liquid precursor for calcium carbonate. *Nat. Commun.* **2018**, *9* (1), 2582.
(101) Wolf, S. E.; Leiterer, J.; Pipich, V.; Barrea, R.; Emmerling, F.; Tremel, W. Strong stabilization of amorphous calcium carbonate emulsion by ovalbumin: gaining insight into the mechanism of 'polymer-induced liquid precursor'processes. *J. Am. Chem. Soc.* **2011**, *133* (32), 12642−12649.
(102) Dai, L.; Douglas, E. P.; Gower, L. B. Compositional analysis of a polymer-induced liquid-precursor (PILP) amorphous CaCO3 phase. *J. Non-Cryst. Solids* **2008**, *354* (17), 1845−1854.
(103) Leukel, S.; Panthöfer, M.; Mondeshki, M.; Kieslich, G.; Wu, Y.; Krautwurst, N.; Tremel, W. Trapping Amorphous Intermediates of Carbonates−A Combined Total Scattering and NMR Study. *J. Am. Chem. Soc.* **2018**, *140* (44), 14638−14646.
(104) Rao, A.; Cölfen, H. On the biophysical regulation of mineral growth: Standing out from the crowd. *J. Struct. Biol.* **2016**, *196* (2), 232−243.
(105) Hunyadi, M.; Gacsi, Z.; Csarnovics, I.; Csige, L.; Csik, A.; Daroczi, L.; Huszank, R.; Szücs, Z. Enhanced growth of tellurium nanowires under conditions of macromolecular crowding. *Phys. Chem. Chem. Phys.* **2017**, *19* (25), 16477−16484.
(106) Sun, S.; Mao, L. B.; Lei, Z.; Yu, S. H.; Cölfen, H. Hydrogels from Amorphous Calcium Carbonate and Polyacrylic Acid: Bio-Inspired Materials for "Mineral Plastics. *Angew. Chem., Int. Ed.* **2016**, *55* (39), 11765−11769.
(107) Raiteri, P.; Gale, J. D. Water is the key to nonclassical nucleation of amorphous calcium carbonate. *J. Am. Chem. Soc.* **2010**, *132* (49), 17623−17634.
(108) Sinn, C. G.; Dimova, R.; Antonietti, M. Isothermal titration calorimetry of the polyelectrolyte/water interaction and binding of Ca2+: effects determining the quality of polymeric scale inhibitors. *Macromolecules* **2004**, *37* (9), 3444−3450.
(109) Lam, R. S.; Charnock, J. M.; Lennie, A.; Meldrum, F. C. Synthesis-dependant structural variations in amorphous calcium carbonate. *CrystEngComm* **2007**, *9* (12), 1226−1236.
(110) Rao, A.; Huang, Y.-C.; Cölfen, H. Additive Speciation and Phase Behavior Modulating Mineralization. *J. Phys. Chem. C* **2017**, *121* (39), 21641−21649.
(111) Rao, A.; Roncal-Herrero, T.; Schmid, E.; Drechsler, M.; Scheffner, M.; Gebauer, D.; Kroger, R.; Colfen, H. On Biomineralization: Enzymes Switch on Mesocrystal Assembly. *ACS Cent. Sci.* **2019**, *5* (2), 357−364.
(112) Cölfen, H.; Völkel, A. Application of the density variation method on calcium carbonate nanoparticles. In *Analytical Ultracentrifugation VIII*; Springer: 2006; pp 126−128.
(113) Liu, J.; Pancera, S.; Boyko, V.; Shukla, A.; Narayanan, T.; Huber, K. Evaluation of the particle growth of amorphous calcium carbonate in water by means of the porod invariant from SAXS. *Langmuir* **2010**, *26* (22), 17405−17412.
(114) Loste, E.; Wilson, R. M.; Seshadri, R.; Meldrum, F. C. The role of magnesium in stabilising amorphous calcium carbonate and controlling calcite morphologies. *J. Cryst. Growth* **2003**, *254* (1−2), 206−218.
(115) Li, H.; Xin, H. L.; Muller, D. A.; Estroff, L. A. Visualizing the 3D internal structure of calcite single crystals grown in agarose hydrogels. *Science* **2009**, *326* (5957), 1244−1247.
(116) Putnis, A. Mineral replacement reactions. *Rev. Mineral. Geochem.* **2009**, *70* (1), 87−124.
(117) Goodwin, A. L.; Michel, F. M.; Phillips, B. L.; Keen, D. A.; Dove, M. T.; Reeder, R. J. Nanoporous structure and medium-range order in synthetic amorphous calcium carbonate. *Chem. Mater.* **2010**, *22* (10), 3197−3205.
(118) Cheng, X.; Gower, L. B. Molding Mineral within Microporous Hydrogels by a Polymer-Induced Liquid-Precursor (PILP) Process. *Biotechnology progress* **2006**, *22* (1), 141−149.
(119) Zhu, F.; Nishimura, T.; Sakamoto, T.; Tomono, H.; Nada, H.; Okumura, Y.; Kikuchi, H.; Kato, T. Tuning the stability of CaCO3 crystals with magnesium ions for the formation of aragonite thin films on organic polymer templates. *Chem. - Asian J.* **2013**, *8* (12), 3002−3009.
(120) Kim, Y. Y.; Hetherington, N. B.; Noel, E. H.; Kröger, R.; Charnock, J. M.; Christenson, H. K.; Meldrum, F. C. Capillarity Creates Single-Crystal Calcite Nanowires from Amorphous Calcium Carbonate. *Angew. Chem., Int. Ed.* **2011**, *50* (52), 12572−12577.
(121) Li, C.; Hong, G.; Yu, H.; Qi, L. Facile fabrication of honeycomb-patterned thin films of amorphous calcium carbonate and mosaic calcite. *Chem. Mater.* **2010**, *22* (10), 3206−3211.
(122) Li, C.; Qi, L. Bioinspired fabrication of 3D ordered macroporous single crystals of calcite from a transient amorphous phase. *Angew. Chem., Int. Ed.* **2008**, *47* (13), 2388−2393.
(123) Kim, Y.-Y.; Douglas, E. P.; Gower, L. B. Patterning inorganic (CaCO3) thin films via a polymer-induced liquid-precursor process. *Langmuir* **2007**, *23* (9), 4862−4870.
(124) Berg, J. K.; Jordan, T.; Binder, Y.; Börner, H. G.; Gebauer, D. Mg2+ tunes the wettability of liquid precursors of CaCO3: Toward controlling mineralization sites in hybrid materials. *J. Am. Chem. Soc.* **2013**, *135* (34), 12512−12515.
(125) Shao, C.; Zhao, R.; Jiang, S.; Yao, S.; Wu, Z.; Jin, B.; Yang, Y.; Pan, H.; Tang, R. Citrate improves collagen mineralization via interface wetting: a physicochemical understanding of biomineralization control. *Adv. Mater.* **2018**, *30* (8), 1704876.
(126) Delgado-López, J. M.; Bertolotti, F.; Lyngsø, J.; Pedersen, J. S.; Cervellino, A.; Masciocchi, N.; Guagliardi, A. The synergic role of collagen and citrate in stabilizing amorphous calcium phosphate precursors with platy morphology. *Acta Biomater.* **2017**, *49*, 555−562.
(127) Davies, E.; Müller, K. H.; Wong, W. C.; Pickard, C. J.; Reid, D. G.; Skepper, J. N.; Duer, M. J. Citrate bridges between mineral platelets in bone. *Proc. Natl. Acad. Sci. U. S. A.* **2014**, *111*, 201315080.
(128) Loges, N.; Graf, K.; Nasdala, L.; Tremel, W. Probing cooperative interactions of tailor-made nucleation surfaces and macromolecules: a bioinspired route to hollow micrometer-sized calcium carbonate particles. *Langmuir* **2006**, *22* (7), 3073−3080.

(129) Nielsen, M. H.; Aloni, S.; De Yoreo, J. J. In situ TEM imaging of CaCO3 nucleation reveals coexistence of direct and indirect pathways. *Science* **2014**, *345* (6201), 1158−1162.
(130) Jiang, Y.; Gong, H.; Volkmer, D.; Gower, L.; Cölfen, H. Preparation of Hierarchical Mesocrystalline DL-Lysine· HCl−Poly (acrylic acid) Hybrid Thin Films. *Adv. Mater.* **2011**, *23* (31), 3548−3552.
(131) Homeijer, S. J.; Barrett, R. A.; Gower, L. B. Polymer-Induced Liquid-Precursor (PILP) process in the non-calcium based systems of barium and strontium carbonate. *Cryst. Growth Des.* **2010**, *10* (3), 1040−1052.
(132) Rao, A.; Cölfen, H. Mineralization schemes in the living world: mesocrystals. In *New Perspectives on Mineral Nucleation and Growth*; Springer: 2017; pp 155−183.
(133) Borukhin, S.; Bloch, L.; Radlauer, T.; Hill, A. H.; Fitch, A. N.; Pokroy, B. Screening the incorporation of amino acids into an inorganic crystalline host: the case of calcite. *Adv. Funct. Mater.* **2012**, *22* (20), 4216−4224.
(134) Kim, Y.-Y.; Ganesan, K.; Yang, P.; Kulak, A. N.; Borukhin, S.; Pechook, S.; Ribeiro, L.; Kröger, R.; Eichhorn, S. J.; Armes, S. P. An artificial biomineral formed by incorporation of copolymer micelles in calcite crystals. *Nat. Mater.* **2011**, *10* (11), 890.
(135) Lu, C.; Qi, L.; Cong, H.; Wang, X.; Yang, J.; Yang, L.; Zhang, D.; Ma, J.; Cao, W. Synthesis of calcite single crystals with porous surface by templating of polymer latex particles. *Chem. Mater.* **2005**, *17* (20), 5218−5224.
(136) Page, M. G.; Nassif, N.; Borner, H. G.; Antonietti, M.; Colfen, H. Mesoporous calcite by polymer templating. *Cryst. Growth Des.* **2008**, *8* (6), 1792−1794.
(137) Nassif, N.; Pinna, N.; Gehrke, N.; Antonietti, M.; Jager, C.; Colfen, H. Amorphous layer around aragonite platelets in nacre. *Proc. Natl. Acad. Sci. U. S. A.* **2005**, *102* (36), 12653−12655.
(138) Chen, H.; Zheng, X.; Li, Q.; Yang, Y.; Xiao, S.; Hu, C.; Bai, Y.; Zhang, T.; Wong, K. S.; Yang, S. An amorphous precursor route to the conformable oriented crystallization of CH 3 NH 3 PbBr 3 in mesoporous scaffolds: Toward efficient and thermally stable carbon-based perovskite solar cells. *J. Mater. Chem. A* **2016**, *4* (33), 12897−12912.
(139) Zhang, W.; Shen, D.; Liu, Z.; Wu, N.-L.; Wei, M. Brookite TiO 2 mesocrystals with enhanced lithium-ion intercalation properties. *Chem. Commun.* **2018**, *54* (81), 11491−11494.
(140) Primc, D.; Niederberger, M. Synthesis and Formation Mechanism of Multicomponent Sb−Nb: TiO2Mesocrystals. *Chem. Mater.* **2017**, *29* (23), 10113−10121.
(141) Dai, L.; Cheng, X.; Gower, L. B. Transition bars during transformation of an amorphous calcium carbonate precursor. *Chem. Mater.* **2008**, *20* (22), 6917−6928.
(142) Aizenberg, J.; Muller, D. A.; Grazul, J. L.; Hamann, D. Direct fabrication of large micropatterned single crystals. *Science* **2003**, *299* (5610), 1205−1208.